Forschungszentrum Karlsruhe

Technik und Umwelt

Wissenschaftliche Berichte

FZKA 6474

Large Muon Tracking Detector in the air shower experiment KASCADE

I. Atanasov[a], W. Bartl[b], H. Bastian[d], C. Büttner, K. Daumiller, P. Doll, B. Hoffmann[d], H. Hucker, K.-H. Kampert[d], H. Kern, H.O. Klages, P. Kleinwächter[c,] D. Martello[d,e], L. Pentchev[a], J. Rachowski[f], F.K. Schmidt[d], G. Rabsch, G. Schleif, H. Skacel, J. Zabierowski[g]

Institut für Kernphysik

[a] Institute for Nuclear Research and Nuclear Energy, 1784 Sofia, Bulgaria
[b] Institut für Hochenergiephysik der Ö.A.W., 1050 Wien, Austria
[c] Forschungszentrum Rossendorf, 01314 Dresden, Germany
[d] Universität Karlsruhe, 76128 Karlsruhe, Germany
[e] Department of Physics, University of Lecce, 73100 Lecce, Italy
[f] Department of Experimental Physics, University of Lodz, 90-236 Lodz, Poland
[g] The Andrzej Soltan Institute for Nuclear Studies, 90950 Lodz, Poland

Forschungszentrum Karlsruhe GmbH, Karlsruhe
2000

Zusammenfassung

Ein Myon Spuren-Detektor für das Höhenstrahlungsexperiment KASCADE

Zur genauen Untersuchung der Myonen, die in hochenergetischen Luftschauern entstehen, wurde im KASCADE Experiment ein großflächiger Spurendetektor aufgebaut. Hierzu wurden 1000 Streamer Tube Detektoren von 4 m Länge gebaut. Der Aufbau des gesamten Detektorsystems wird beschrieben. Es werden Methoden beschrieben, die es erlauben, die Geometrie und die Winkelauflösung des Detektorsystems zu bestimmen.

Abstract

A large area Streamer Tube (ST) detector, located within the KASCADE experiment, has been built with the aim to identify muons from extensive air showers (EAS) by track measurement under more than 18 r.l. shielding. 1000 ST detectors of 4 m length have been built and tested. Extensive tests led to many improvements in the detector construction. The construction of the whole detector together with its electronic is presented. The methods of precise determination of detector geometry as well as tools for detector angular resolution derivation are discussed.

corresponding author: doll@ik1.fzk.de

Table of contents

1 Introduction

Ultra high energy (UHE) astrophysics deals with the investigation of UHE cosmic ray particles (above 10^{15} eV), which interact with the nuclei of the atmosphere and create an extensive air shower (EAS). However, at UHE their flux is much below $10^{-5}\mathrm{s}^{-1}\mathrm{m}^{-2}$. Therefore, instead of satellites in space, ground based experiments of large detection area must be used. To understand the nature of the UHE particles it is compulsory to measure as many components as possible of the cascade developing in the atmosphere. Particularly important is the measurement of the muon component of the EAS, because some of the muons reaching the observation level carry information about very first interactions at the top of the atmosphere. For large distances from the shower core individual muon tracks point to the height of the muon production and help to identify the nature of the primary UHE particle. Monte-Carlo calculations show that by means of the production height parameter, for a good statistics of showers, primary particles like iron nuclei (Fe) can be separated from light ones, like hydrogen (p). In particular, the investigation of muon arrival times and their angle-of-incidence with respect to the shower axis, as Monte Carlo calculations show, can reveal the nature of the UHE primary cosmic ray particles.

As investigated in [1], [3], [5], [6] the combined analysis of those two observables (which may be correlated) can improve the mass discrimination of the primary, as compared to the analysis of one of these quantities separately, observed with equivalent accuracy. Therefore, use of tracking and timing devices, such as in [2], has sure advantage. The standard reconstruction of the MPH by triangulation involves only the radial component of the angle between the shower axis and the muon track [4].

As an extension to the KASCADE EAS experiment [7] a large area streamer tube (ST) Muon Tracking Detector (MTD) was put into operation. KASCADE at the *Forschungszentrum Karlsruhe* has been taking data since 1996, measuring various shower parameters with the 200×200 m^2 scintillator array and a central detector, consisting of hadron calorimeter and muon detectors. The new MTD of about 500 m$^2\cdot$ sr is intended to track the muons created in the EAS. In addition, it will enhance the capability of KASCADE in measurement of the muon multiplicities and their lateral distributions.

The MTD will also allow to perform systematic studies on cosmic ray muons like those carried out by O. C. Allkofer et al. [8].

Main parameters of this ST detector, as seen at the early prototyping stage, were described in [9]. The present paper is a detailed presentation of a built detector system. After brief presentation of the purpose of the detector, the specially developed ST's will be described together with the elaborate tests after production and their results. Next,

the presentation of the complete detector system, its geometry and readout electronics will follow. And finally, the methods of investigation of detector angular accuracy will be presented.

In the past, various tracking detectors for measuring cosmic ray particles have been put into operation either on the surface of the earth [12], [13], [14], [15] or deep underground [10], [11], [16]. The surface arrays emphasize the aspect that position sensitive detectors which measure the angle of each track, may be used to improve the precision in the measurement of the primary particle direction, since the directions of muons are much better correlated with the primary direction than are the directions of electrons [14]. Multiwire proportional chambers were also operated [13], to investigate particle density distributions close to the shower core. Improved identification of particles in air showers was studied using tracking chambers and a thin absorber [12]. Tracking modules made from planes of ST's have been applied to the observation of extensive air showers in the PLASTEX experiment [15]. Very large ST detectors or Geigertube counters have been set up in the Gran Sasso Tunnel [10], [11], and Frejus Tunnel [16]. All three detectors can be defined as underground observatories with the main objectives of studying very high energy muons and neutrinos from stellar collapse and searching for point-like sources of gammas and neutrinos of very high energy.

2 Some detector applications

Introduction of the large muon tracking detector (MTD) into KASCADE experiment has significantly widened the multiparameter EAS analyses capabilities. The redundancy of information can be used to find out systematic biases in the interpretation of the data.

As a tracking detector, the MTD is able to identify the directions of muons, which for distances close to the shower axis can be used as an independent determination of shower direction. Consider for this purpose muon bundles with almost parallel tracks. For the larger distances to the shower axis the direction of the muon track points towards its origin, high in the atmosphere. The reconstruction of the muon production height (MPH) distribution, related to the nature of the primary UHE particle, is a primary goal of this detector. The triangulation of the muons may also help to investigate the transverse momentum distribution of muons for constrained primary particle energy and production height.

Extensive Monte-Carlo calculations have been carried out to investigate the possibility to derive from the muon angle the production height of the muon. Supported by simulations

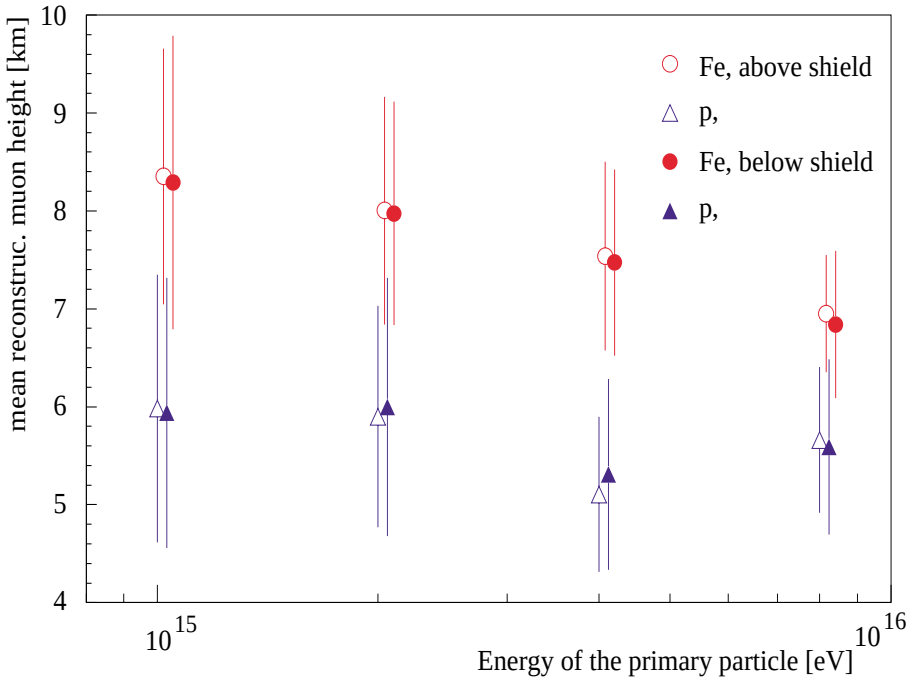

Figure 1: Mean MPH reconstructed by simple geometrical means for Monte-Carlo simulated showers initiated by proton and iron primaries. Errors represent the spread of the distributions. The influence of the tunnel shield (18 r.l.) on reconstruction is shown.

the measured MPH can be used to classify the showers into those which originate from heavy primary particles, like iron nuclei (Fe), and those from the light ones, like hydrogen (p). Fig.1 reveals the energy dependence for such a possible separation.

As it is seen in fig.2, heavy primary nuclei produce a good fraction of muons already at high altitudes. By means of the simulations with the CORSIKA [33] program it has been found, that the muons produced at different atmosphere depth exhibit significantly different angular spreads at the observation level. While the array data provide, besides the shower core position and shower direction, integral parameters like electron size and muon size, these additional parameters, which result from the triangulation of the muon tracks with respect to the shower axis, can be included in a multiparameter analysis.

As pointed out above, a ST tracking detector, being capable of independent determination of the shower direction, can be used in combination with the scintillation array to improve the overall angular resolution of the total KASCADE experiment, especially for low shower sizes, where the angular resolution of the array deteriorates. This will be discussed in the following sections.

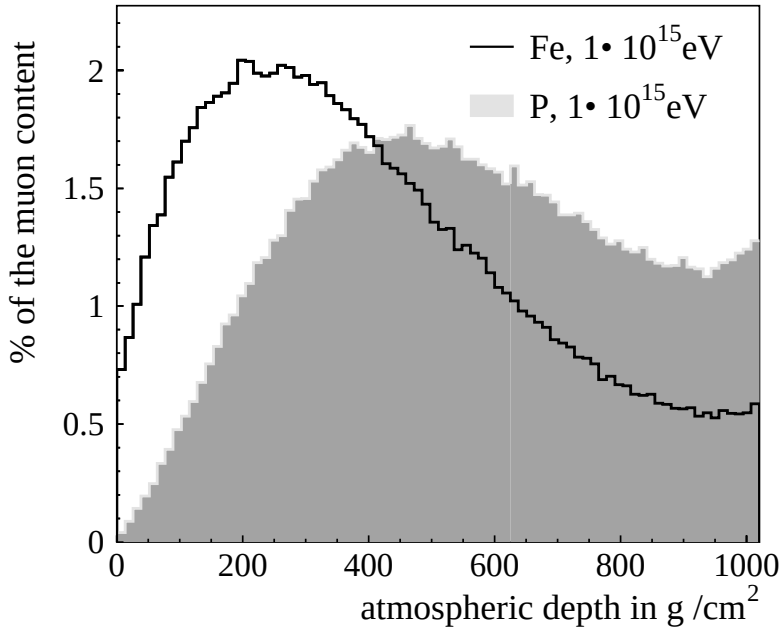

Figure 2: Simulated MPH distribution (muon content per histogram bin = 12.5 g/cm^2) in air showers initiated by proton and iron primaries.

However, the MTD is also a large area detector, which can be used for studying the muon densities and their lateral distribution function close to the shower core. The internal structure of muon bundles can be analyzed.

3 Serial tests procedure

Preparational studies [9, 17] with various commercial STs [18, 19] and custom-made tubes [20, 21] for the air shower experiment KASCADE did indicate that this type of detector [22] is well suited for particle density measurements in air showers or track measurements of penetrating particles.

After investigating different types of streamer-tubes employed in high energy physics experiments, we had to find a structure to build several hundreds of square meters of streamer-tubes of very reliable quality. Only good reliability can compete with large area scintillators which are commonly used in air-shower experiments.

Different groups having experience in producing these type of detector had been contacted as possible supporters. However, it was necessary in the prototyping phase to introduce as many improvements as possible, by constantly testing assembled chambers. Because of future considerations of employing gas detectors in EAS studies in a large quantity, a new company was set up (WATECH) by one of the authors [23], who was familiar with the technique of producing conductive PVC comb profiles. Conductive plastics cover a very interesting field of research and their application in the present detectors required extensive investigations [23].

Together with this company we investigated, for example, the high resistive cover of the open comb profiles [24]. In order to reduce the dark current in the chambers we replaced the anode wire material by high quality copper-beryllium wire. We employed 100 μm diameter high quality wire tempered and straightened with approximately 0.3 μm of silver, with a copper flash under the silver [25]. The first leak tests as well as the conditioning of the detectors have been made on the site of the factory using pure carbon-dioxide as chamber gas.

Concerning the detector dimensions, the ST chambers have been built, housing 16 anode wires in 2 cathode comb profiles, extruded for 8 parallel ST cells of 9×9 mm^2 cross section and 4000 mm length. For the comb profiles the high resistivity PVC of well defined conductivity of 100 kΩ/square was obtained from very clean PVC by doping it with carbon powder before extrusion [23]. To close the field around the anode wire very effectively [24] when applying negative HV to the cathode profiles, for the cover of the comb profiles a bakelit sheet of about 10^{11} Ω/cm^2 was employed.

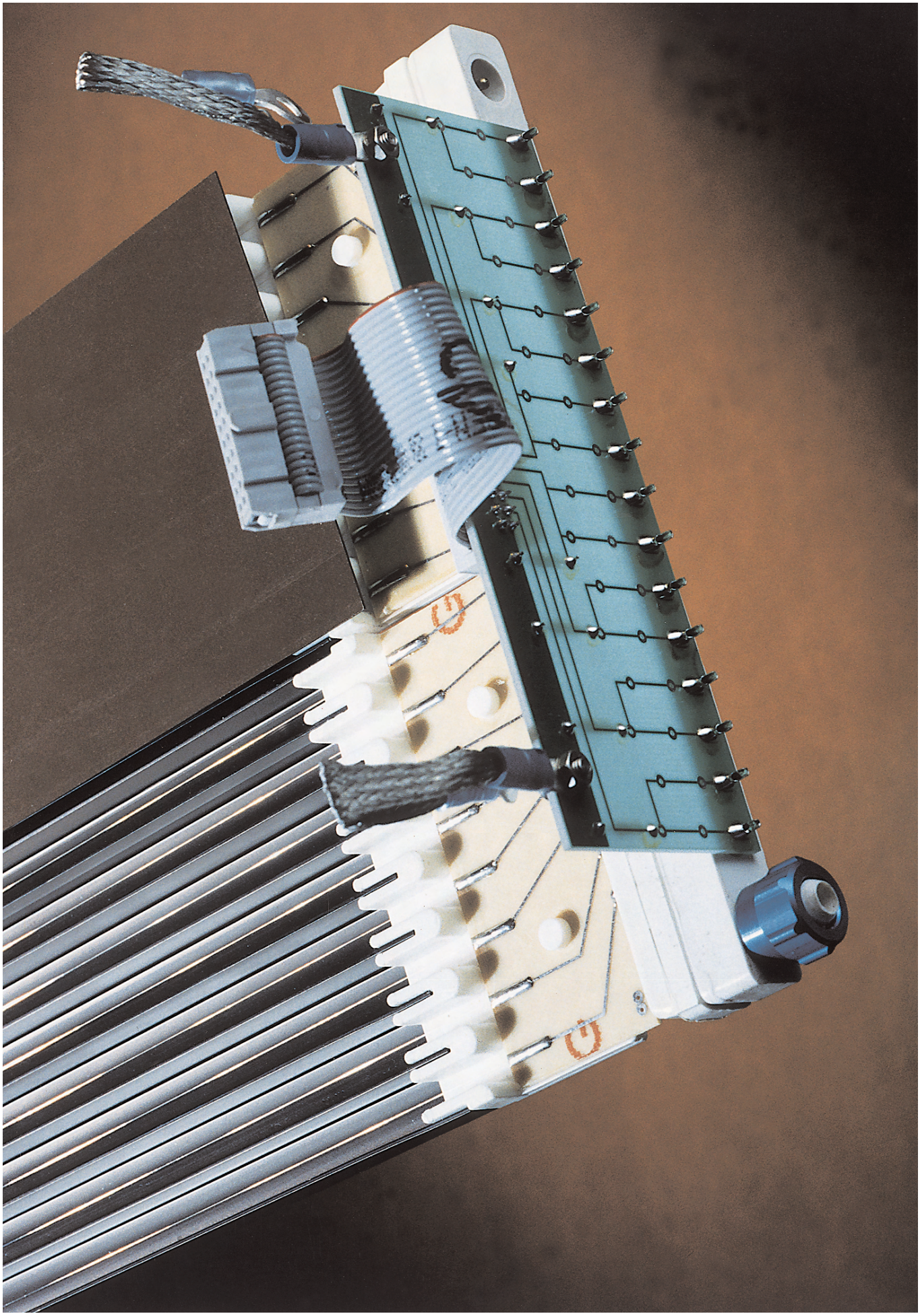

Figure 3: detailed view of opened ST with installed adapter board.

The geometry of the ST cell was required to vary less than 0.1 mm. Onto each comb profile end-pieces were glued, which carry the printed circuit boards, onto which eight anode wires were soldered.

The wires are supported every 500 mm along their length of 4000 mm. The wire tension before soldering was adjusted according to the room temperature of the detector assembling hall around 3 N at 20^o, taking into account the much larger expansion coefficient of the PVC structure. The copper-beryllium wire has an expansion coefficient about 3 times smaller than the PVC material. Therefore, a given wire tension of 3 N at 20^o varies by ± 0.22 N for $\pm 5^o$ of the operation temperature change in the tunnel. Correspondingly, the wire sagging between the spacers varies around 42 μm by ∓ 9 μm for $\pm 5^o$ of temperature change.

These comb profiles, together with the wires, were slided into PVC envelopes, which were sealed off with endcaps exhibiting connectors for anode wires, high voltage and gas. The outer width of such a ST chamber with 16 wire cells amounts to 168 mm (fig. 3).

When the detectors arrived at the *Forschungszentrum Karlsruhe* they were checked for mechanical damage and then individually tested for leaks. Each chamber was put under 20 cm of water equivalent overpressure and closed off for 2 hours. Outside pressure and temperature were monitored to correct any change in the water column for these environmental variations. From the real losses in gas the effective loss in units of chamber volumes per year was calculated, normalized to an operation overpressure in the air-shower experiment of 5 millibar.

A compilation of the leak rate for all 1000 chambers shows that 85% of all chambers exhibit a leak rate of less than one detector volume per year. The remaining detectors exhibit also a tolerable leaking. Therefore, with a gas flow of 0.5 l/h we exchange the full volume in 3 weeks, which is enough to keep any possible contamination from the outer air sufficiently low. Also with respect to the low rate of penetrating radiation in the shielded tunnel in the KASCADE experiment a slow gas exchange is tolerable.

After the leak test the detectors were put on tables in groups of 12 and flushed in parallel with an isobutan/argon gas mixture. This flushing replaced over one weekend the carbon-dioxide. Fig.4 shows the count rate plateau for various gas settings.

The results in fig. 4 were obtained by measuring the integral rate in the pulse height spectra from a ST, however, gated with a plastic scintillator telescope. We continued to test the chambers, with the lowest isobutan admixture, to avoid during the conditioning phase the build up of organic radicals on the detectors electrodes. On those test tables the detectors were read out by a prototype readout chain (see section 5) recording the hits on the wires and on pick-up strips, which have been arranged perpendicular to the wires, with

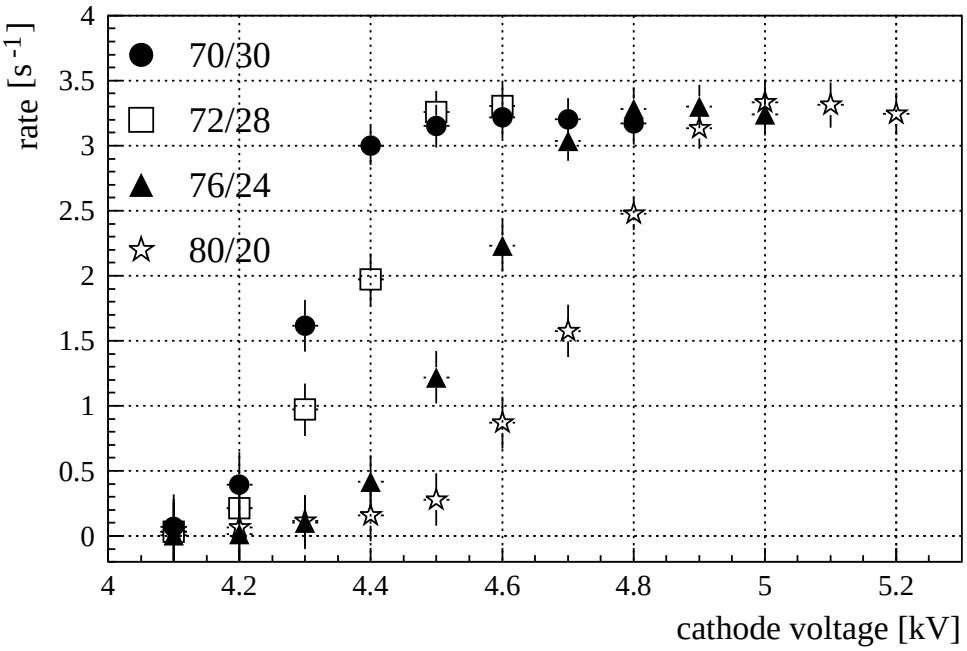

Figure 4: Count-rate plateaus for various isobutan/argon gas mixtures. Numbers quoted are in volume percent.

a pitch of 20 mm and width of 18 mm. Also the amplitudes on the anode wires caused by the cosmic ray particles were recorded. Actually the STs were brought always to the same operation voltage in the plateau region (see fig.4) and data were taken as presented in fig.5.

This figure shows the variation of the mean pulse height across a module of 2×4 m^2 consisting out of 12 chambers and 192 perpendicular strips of 20 mm pitch. After 2 hours of data taking a full survey of 12 STs was obtained. For the observed variation of the mean pulse height the following factors may be responsible. We know, that the fresh detectors exhibit spurious discharge signals of various amplitudes. This has an influence on the mean ADC values shown in the picture because the threshold settings of the comparators in the readout chain (see section 5) can be equalized only with a finite precision.

To investigate the homogenity of the detectors in closer regions of several strip pitch units, the wire amplitude spectrum was off-line divided into components recorded in coincidence with varying number of influence strips as shown in fig. 6. The varying number of influence strips, mainly determined by the spatial extension and orientation of the discharge in the wire cell is called the cluster size. The integral intensities in this different wire amplitude spectra follow approximately the geometrical spread of the influence charge on

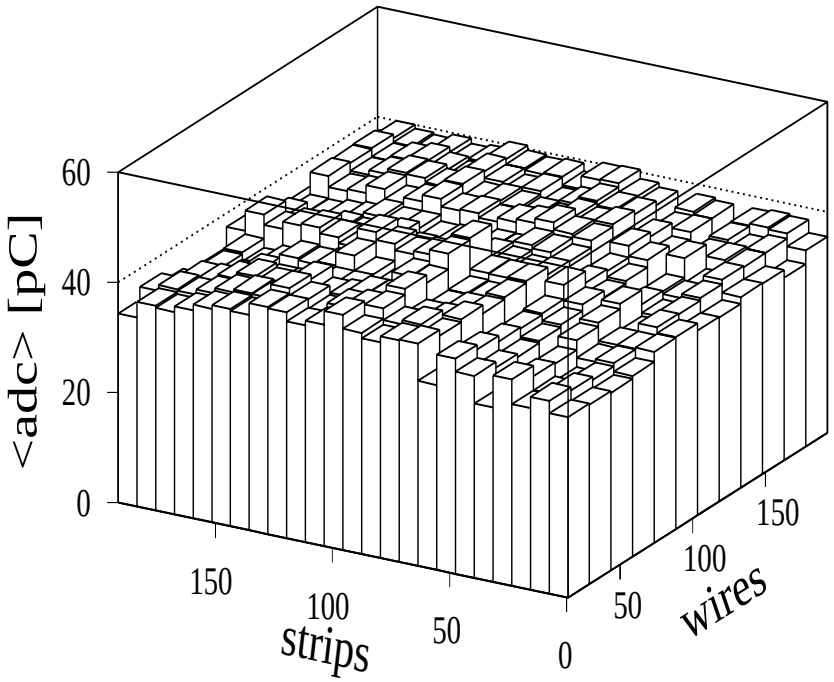

Figure 5: Variation of the mean pulse height across a module of 2 × 4 m^2 consisting out of 12 chambers housing 192 wires and 192 perpendicular strips.

the strips and depend also on capacitive coupling through the bakelit sheet and chamber envelope.

The production and test period for 1000 STs did last for several months. During this period changes in the gas mixture and operation temperature in the laboratory and gas pressure did occur. To obtain a survey of the mean pulse height quality of all chambers we did correct their anode wire pulse height distribution for these parameters, which had been monitored during the runs. In fig.7 the distribution of the mean anode wire pulse height is presented. The spread of this distribution may be due to operational variations in the recurring setup and variations in the chambers geometry. During the first measurement, the fresh detectors exhibited varying integral count rates due to the incomplete conditioning. This rates have also been corrected for the operation conditions.

The operation of assembled towers was observed over long periods. As figure 8 shows, the detectors experience in the tunnel, over a period of one year, temperature changes from 15^o to 25^o (almost no day/night variations) and pressure changes from 990 to 1040 mbar. These parameters influence the operation of the gas detectors. In the figure the behavior of the upper module of tower 3 (192 wires) during the period 31.5.1998 (day 151)

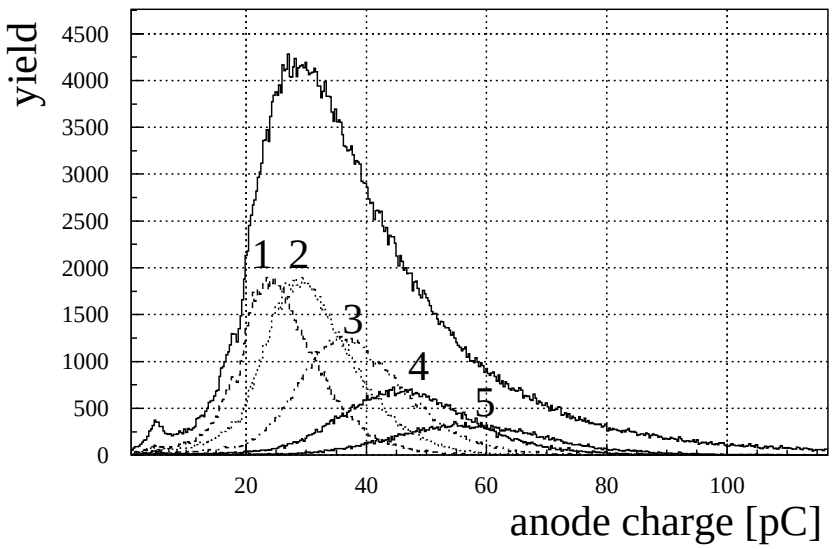

Figure 6: Anode wire amplitude spectrum divided up into contributions from increasing cluster size (1 to 5) on the pick-up strips placed above the chamber.

to 30.4.1999 (day 485) is shown. The temperature and pressure changes modify also the amplitudes in the STs, which are continuously recorded.

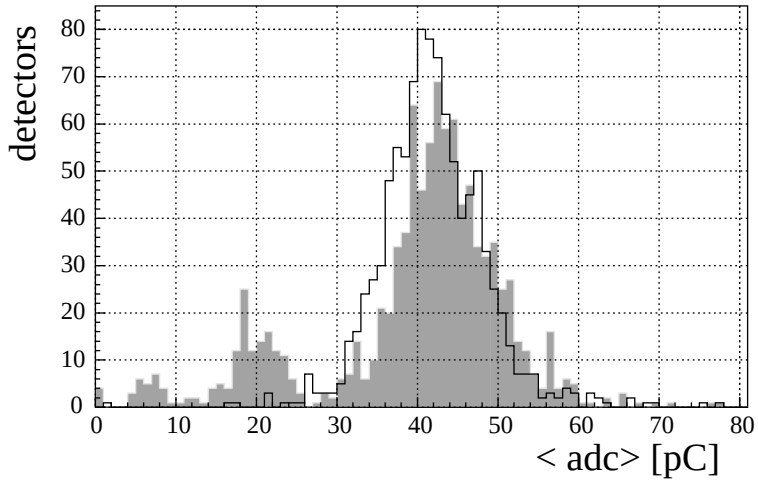

Figure 7: Variation of the mean anode wire pulse height for 1000 chambers before (grey) and after (solid line) corrections for different operation conditions.

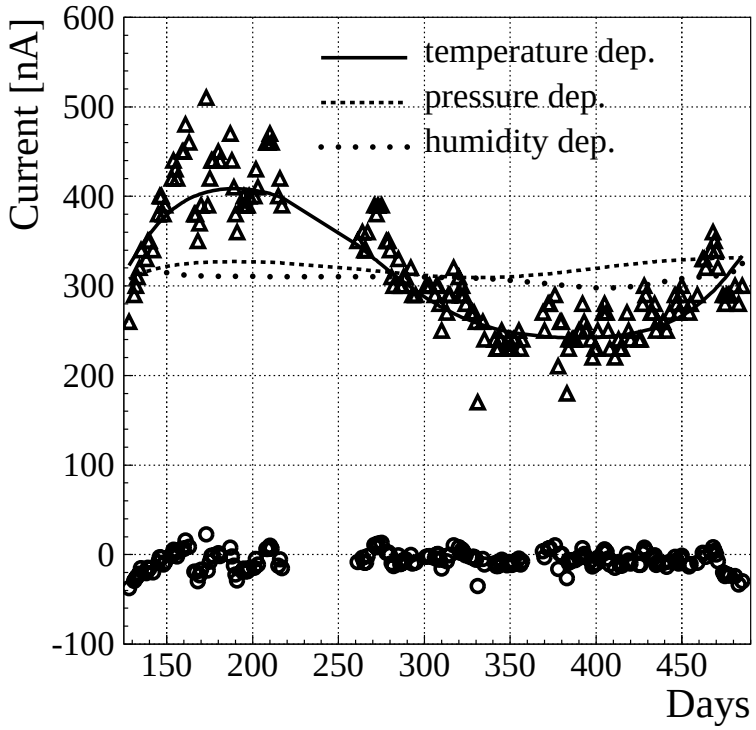

Figure 8: This plot shows the current (△) drawn by upper module of tower 3 and its dependence on temperature, pressure and humidity. Constant current values (○) are reached after correction for these dependences (shifted in the plot by -330 nA).

4 Description of the detector

The ST Muon Tracking Detector is located within the KASCADE EAS experiment (fig. 9) in the tunnel buried in the ground under a shielding of 18 r.l., made out of concrete, iron and soil. A multilayer of 6 iron plates of 3 cm thickness, separated each by 5 cm sand, provides a good absorber for a large fraction of low energy electromagnetic particles, thus enhancing the tracking capability and identification of the muons with an energy above 0.8 GeV.

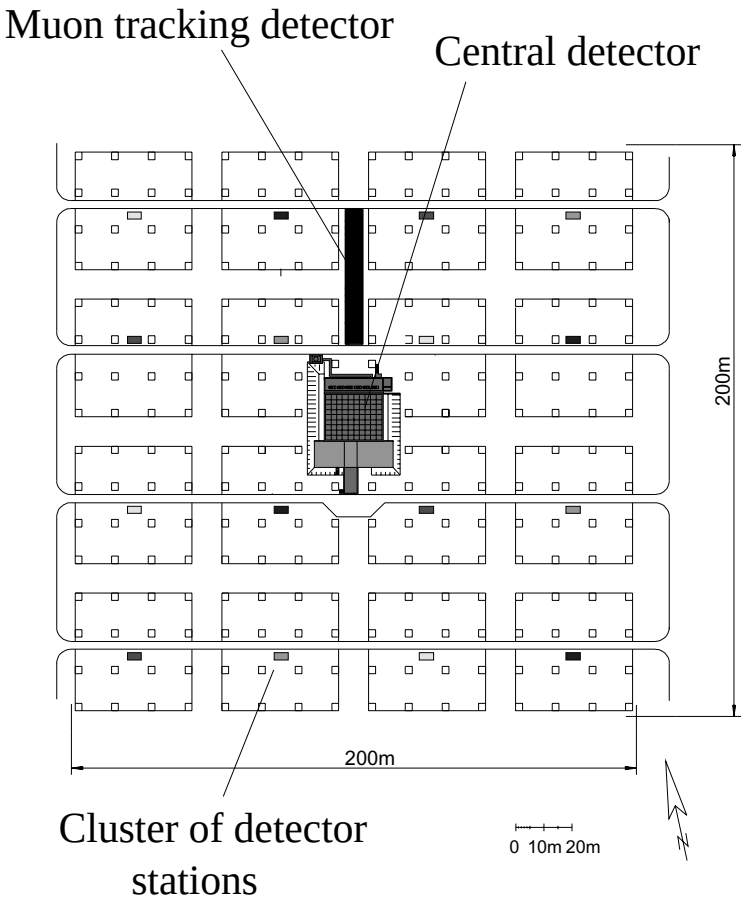

Figure 9: Layout of KASCADE EAS experiment.

The location of the tunnel supports the detection of muons around the central detector, which houses other muon detectors, operating at different muon energy threshold. A cross section of the detector tunnel of 5.4×44 m^2, together with an array detector station located nearby, is shown in fig 10. The STs described above are used in, so called, *modules*. Four modules, three positioned on horizontal planes and one arranged vertically, form a muon

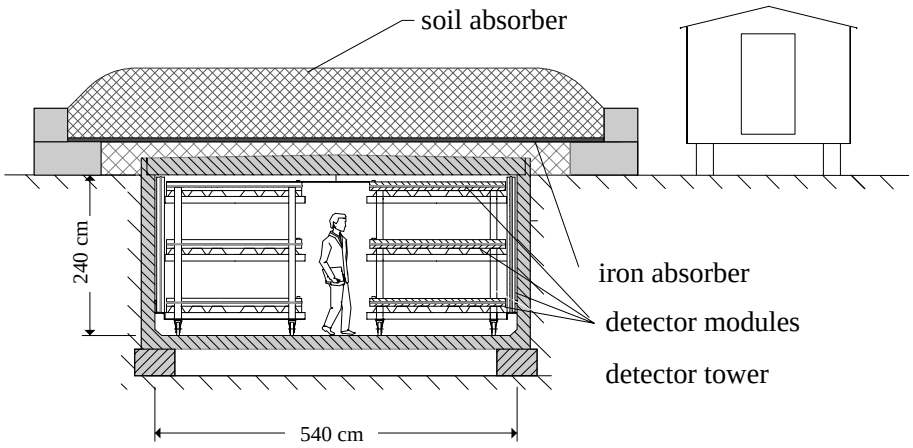

Figure 10: Cross section of the muon detector tunnel.

telescope called *detector tower*. The whole detector consists of 16 towers arranged in two rows. In fig.10 two such towers are shown. The 3-dimensional structure of two towers, drawn with the data sample of 250 000 hits in the detectors is shown in fig.11. The photo of the complete muon detector system in the tunnel is presented in fig.12.

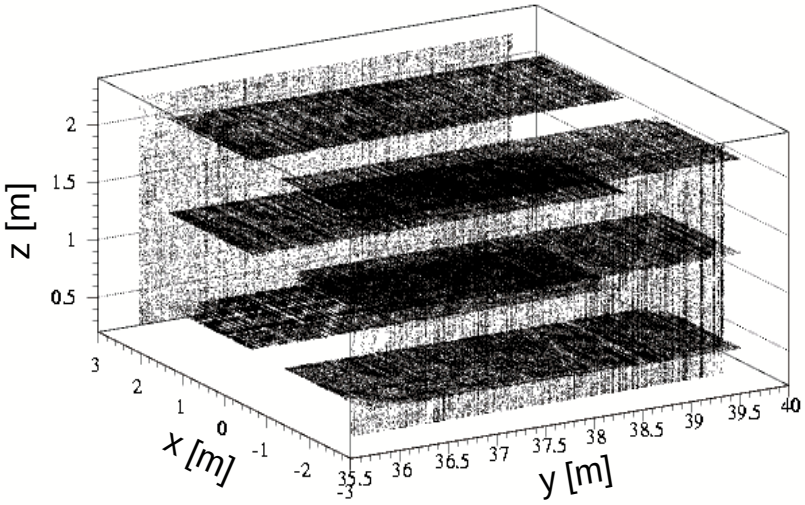

Figure 11: Structure of two towers plotted with the data of 250000 hits.

Figure 12: Streamer tube MTD in the tunnel.

4.1 Detector module and the tower

A detector *module*, of the size 2×4 m^2, consists of a set of 12 ST chambers, as described in section 3. Above the ST chambers there is a layer of a rigid polyester foil of 75 μm thickness with evaporated aluminum strips of 20 mm pitch (18 mm width) and 2 m length, perpendicular to the wires. Another layer of such foil is mounted below the tubes but with strips oriented diagonally (60^0). These *diagonal strips* are made out of the same strip material but 2 strips are connected on the readout side. The total resistivity of a *perpendicular strip* is 35-40 Ω and amounts up to 25 Ω for a diagonal strip pair, depending on the length. The strip material which is called a Steiner Film [26] has thick aluminum strips (about 0.1 mg/cm^2) evaporated on the polyester foil by means of a special technique.

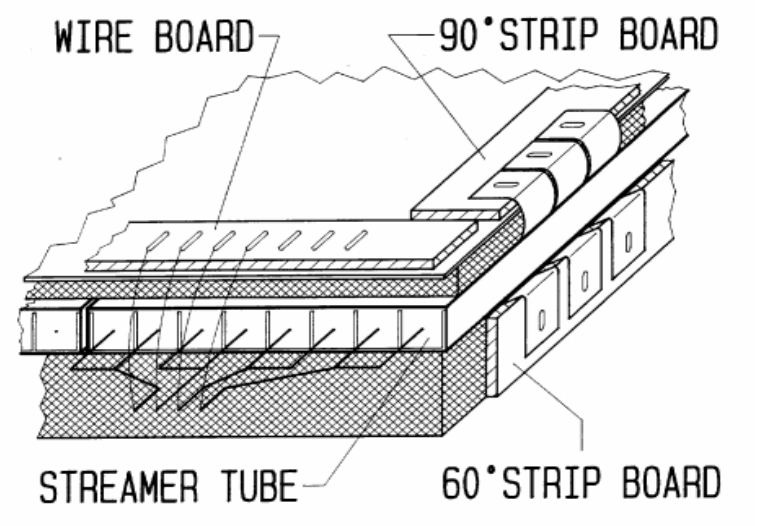

Figure 13: Schematic module design. The PVC boards for fixing signal outputs from wires, perpendicular and diagonal strips are shown.

The electrical contact with the strips is achieved by screwing a broad silver coated ring together with the foil onto a rigid PVC board (shown schematically in fig.13). Onto those boards further intermediate printed circuit boards are soldered for enabling connection to the readout electronics. In the same figure it is shown schematically, that two neighbouring wire cells are combined, thus giving four wire signals out of one 8-cell profile.

The chambers together with the strip foils are sandwiched between two boards of high density styrofoam (25 mm from above and 50 mm from below) and are resting on a thin (0.7 mm) steel structure. For the readout electronics every module is a source of 96 wire

signals, 192 perpendicular and 96 diagonal strip signals. Combination of those signals enables reliable location of the particle hit in X-Y (wire-strip) plane.

A muon tracking telescope, a basic subunit of the full detector, is built out of 4 detector modules in a form of a *tower*. Three modules are put horizontally, spaced by 820 mm from wire plane to wire plane and one module is arranged vertically. The latter module allows to investigate very inclined showers, which could either result from UHE cosmic ray particles or from neutrinos. Additional detector modules and/or absorber planes can be installed in between the horizontally arranged modules.

The gas supply system is arranged as follows. The gas leaves the gas mixer unit and is divided into 16 channels. Such a channel supplies one tower, where the gas runs in series through all chambers of the top module, then the middle module, next the bottom one and, finally, the wall module. With a gas flow of 0.5 liter per hour, the gas in one tower is exchanged after about 20 days which is adequate with the small leaking of the detectors and small radiation load in the shielded tunnel. The total length of the gas system for all ST chambers in series amounts to almost 200 m for each tower.

5 Readout and data acquisition electronics

We are using a chain type of readout system, commonly used with the large scale ST detectors [27, 28]. The readout electronics can be subdivided into three groups. The first group in the readout structure is the front-end electronics, consisting of boards for 32 inputs, mounted to the detector modules and acquiring signals from wires and strips. Each module supplies 96 wire and 288 strips (192 perpendicular and 96 diagonal) signals. The total number of readout channels in 16 detector towers amounts to 24576.

Front-end board design follows the general functionality of the ones used by other groups [27, 28], being in principle a shift register with amplifiers and discriminators in the input channels. However, the circuit implementation and the layout is of our design, matching our detector in the best way, and it will be described in more detail below. The front-end boards generate digital signals from the strip and wire signals, and an analog sum (ANOR) of the combined wire signals for 4 ST chambers. The ANOR spectra are very useful information in addition to the hit pattern.

Each module requires 3 *wire boards* and 9 *strip boards* for readout. The boards for two module combinations (bottom + middle or top + wall), 24 boards each, are interconnected in series by means of a common 20-conductor ribbon cable, thus forming a serial readout chain structure.

Such a chain is connected to the second group in data readout structure, the dedicated intermediate electronic module, called *Splitter Board* (SB). Four of such SBs occupy one crate and provide the interface for two detector towers. These SBs are of our custom design, however they are functionally compatible with CAEN SY480 modules, in order to match the CAEN C267 STAS (Streamer Tube Acquisition System) CAMAC controllers, used in our setup.

One CAMAC and one VME crate contain the third group of the electronics structure. The CAMAC crate contains four C267 STAS modules plus several 2249 LeCroy ADCs for the analog wire signals (ANOR). The VME crate communicates with the CAMAC system via CES 8210 CAMAC Branch Driver and houses trigger electronics [31], controller for CAEN High Voltage System, ADC for analog quantities like temperature, gas pressure and flow, and the transputer based controller (TVC) [32] for communication via optical links with the central host in the KASCADE data acquisition system.

5.1 Front-end boards

The front-end readout boards for our tracking detector follow the general 32 channel architecture, developed by SGS Thomson [29] as IP32 cards and used in many applications with ST detectors [27, 28]. Subdivision into 32 channels per board matches our detector requirements. The idea of the front-end electronics board for chain readout consists of conversion of each analog signal from wires or strips, which exceeds predefined threshold, into digital binary information ("hit" or "no hit"). This binary information, under certain triggering conditions, is loaded in parallel into a 32 bit long shift register. Connecting 24 boards in a chain, as in our case, creates a 768 bit long register, from which data is shifted out, via the bus, with the clock frequency of 1 MHz into the STAS Controller during readout cycle. The physical length of a 24 boards chain amounts to 24 m. Along this path a very good grounding must be provided. Signals from wires are normally about 5 times larger and of the opposite polarity than signals from strips, which are positive pulses. Therefore, two types of boards were developed: for wires and for strips.

One analog channel of our strip board is shown in fig.14. Our design does not use D779 hybrid chip as in case of IP32, therefore, no refresh signals are necessary. However, the analog part of the board is made in SMD technique, what makes the layout more compact and better protected against pick-ups and cross-talks of various origin. The circuit components were selected under the aspect of maximal reliability and minimal cost. A typical positive strip signal has 20 ns rise time and is 50 ns long at the base. These pulses are amplified $\sim$ 20 times in T1-T2 amplifier and presented to the inverting input

of the discriminator. MAX908 from MAXIM [30] combines the discriminator and one-shot functions. This is a single supply device, therefore, the zero at discriminator input is shifted to the $V_{ref} = 2.45$ V level. Threshold voltage can be derived either from the voltage supplied over the bus lines from SB or created locally on board. A group of 8 channels has a common threshold value, adjusted via trimpot on board. The output of the one-shot, logical pulse 4 - 6 μs long, depending on the time-over-threshold value of the input pulse, is presented to one of the parallel inputs of the shift register, built of 74HCT166 chips.

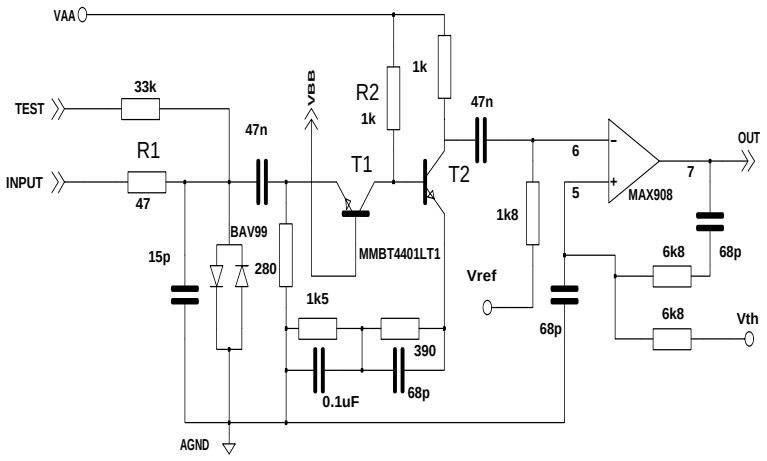

Figure 14: Schematic diagram of the analog part of strip readout circuit. MAX908 comparator serves as a discriminator and one-shot.

The circuit components were chosen in such a way, that this pulse is generated only when time-over-threshold at the discriminator's input exceeds 30 ns. This gives a protection against short spikes of different origin. A logical "OR" of all 32 discriminator output pulses on board forms a 'Digital OR' (DIGOR) signal. It is used internally for loading shift register (via SHOT-LOAD signals coincidence similar to the one described in [28]) and is available for external use outside the board (e.g.. for triggering purpose).

The analog channel for the wire board differs from the one shown in fig. 14 mainly in the amplifier configuration. Transistor T2 is there in an emitter follower configuration (we do not need to invert the signal and the gain can be 5 times less). Also resistors R1 and R2 have different values: 180 Ω and 1.8 kΩ respectively. On the wire board an analog sum of all input signals is produced (ANOR). This ANOR signal is digitized in CAMAC LRS 2249 ADCs and obtained spectra are very useful information, in addition to the hit pattern. ANOR is an output of a summing amplifier circuit shown in fig.15. The input resistors are

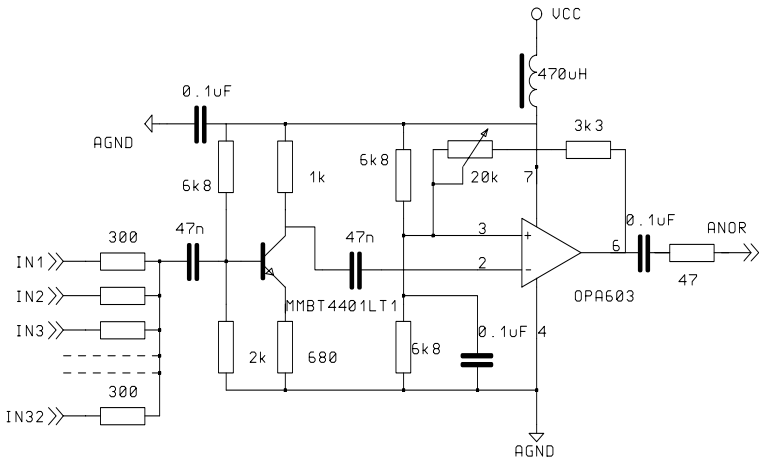

Figure 15: Summing amplifier for analog wire signals.

connected straight to the wires of the chamber. The OPA603 with its 1000 V/μs slew rate and high output current (150 mA peak) is well suited for this application.

The power supply VCC = 10 V is taken from the bus (supplied by SB) after LC filtering. The same VCC is used on board to produce (7805 regulator) VDD = +5 V, a digital power supply voltage for all digital circuits.

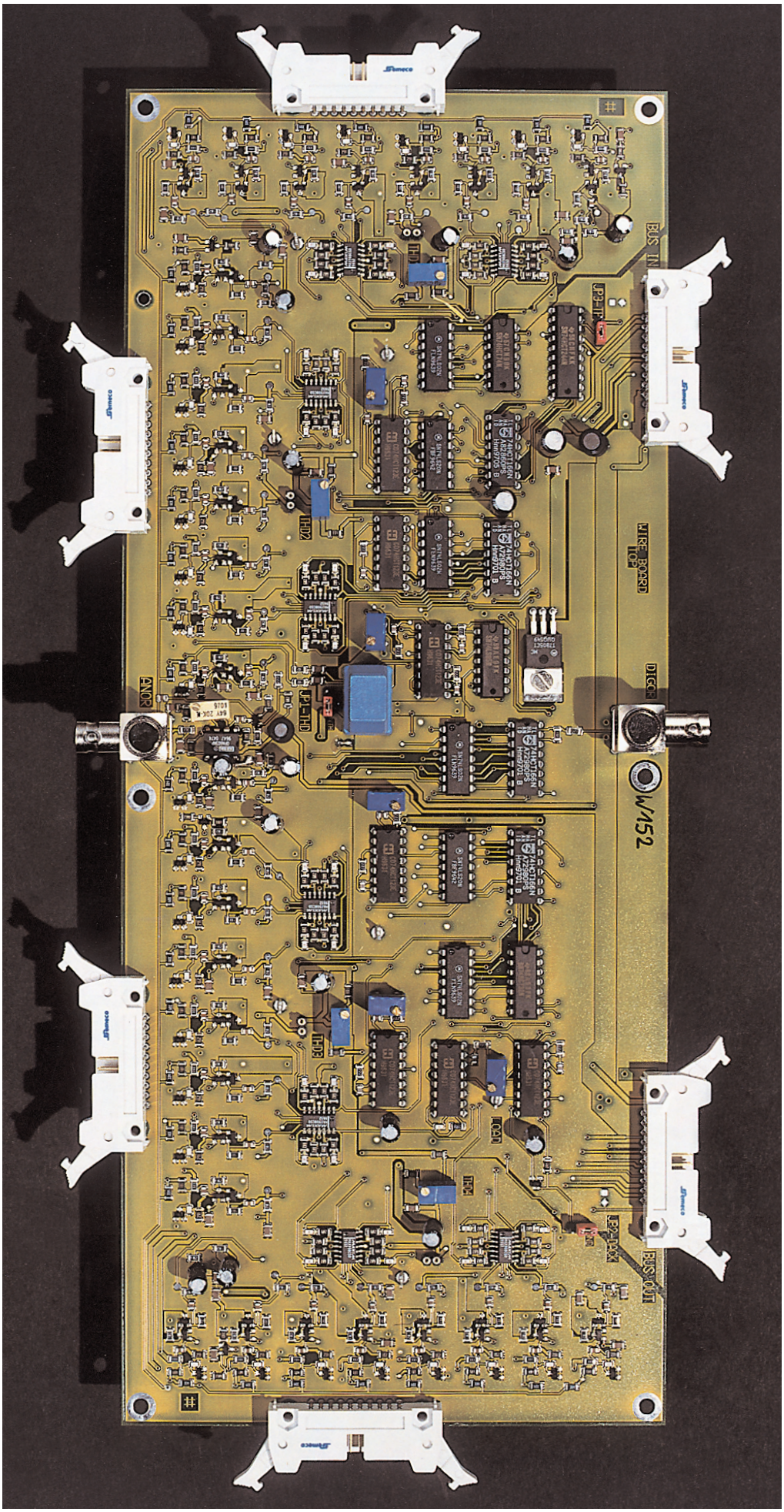

Figure 16: Front-end board for the ST Muon Tracking Detector.

The best possible separation of power supplies and grounds between analog and digital parts on the board is a crucial requirement in ST front-end electronics. The quality of this separation sets the lower limits on the possible threshold values, having an overall consequence in the obtained efficiency of muon registration.

The layout of our board was designed in such a way, that one obtains maximum separation. Areas containing analog and digital circuits are well separated from each other. Also electrically, analog (AGND) and digital (DGND) grounds, as well as power supply voltages: digital (VDD) and analog (VAA), are connected in one point only through 6.8 μH inductive coils. The analog area is distributed over three edges of the board (edge connectors to the detector) - see fig.16 - while the digital part, related to the shift readout, is confined to one side only. Moreover, the lengths of the tracks conveying the bus signals on the board is significantly shortened in comparison with the previous designs, by fixing the shift direction on the board. In our case bus input and output connectors are dedicated. This solution allows extension of the bus length even beyond 24 boards without problems also at 4 MHz clock frequency. Bus connectors are situated as close as possible on one of the long edges of 345 $\times$ 140 mm^2 front-end board (see fig.16).

As a result of a careful design boards are very "quiet" what allows to work with effective thresholds below 1 mV. However, in each case the working threshold has to be optimized for minimum cluster size (which means the number of influence strips) without loosing the efficiency. These threshold values are usually higher than the minimum ones derived from signal/noise considerations.

The test and tuning of the 850 strip and wire readout boards were performed using a program (Qbasic) on a PC. By means of a special interface board the program provided the steering and test signals via the parallel port of the PC.

For testing the shift registers a programmed 8-bit word was shifted through a chain of a given number of boards many times, and each time at the output compared with the input word.

For testing the many amplifier channels the test-even and test-odd lines available on the boards were employed. Usually along these lines the monoflops are triggered for all 16 even or 16 odd channels of one board. The amplitude range on these 16 parallel lines could be varied to compare the signal ranges.

By tuning the threshold voltages (V_{th}) all comparators on the boards were put to starting values, which had to be adjusted after the boards had been mounted to the detector module, because of modified ground loop currents. After the tuning of the threshold voltages the timing of the LOAD and the delay of the CLOCK-INHIBIT signals were set on the oscilloscope. All test and tuning results were written into a protocol.

5.2 Triggering

For the purpose of triggering of the ST tracking detector a custom made Trigger Unit (TU) was designed. It is a detector specific modification of the module used for KASCADE scintillator array, which is extensively described in [31].

The two trigger modes are possible: *internal* and *external* one. For internal triggering a multiplicity combination of DIGOR signals from bottom wire boards of all towers is used. Any value of this multiplicity in the range from 1 to 48 can be preset by software. As external trigger sources other KASCADE detectors like the scintillator array, the top cluster or the trigger plane are used. Upon fulfillment of either of the triggering conditions the TU sends an EVENT signal to the TVC and the readout procedure is started.

One of the important tasks of the TU is the generation of the *Time Label* (TL) for each event. Such TLs are generated also in other parts of the KASCADE experiment and are used by acquisition software to build an air shower event from data supplied by various detectors (central event builder). With every event an actual time is also being stored. It is derived from a central GPS controlled clock system of KASCADE at the start-up of the MTD and then, incremented locally in the TU by centrally distributed 1 Hz precise clock signals. With the TL every trigger absolute time is recorded with 200 ns precision.

5.3 Event handling

Whenever a trigger condition (see 5.2) is fulfilled in the Trigger Unit (TU), an EVENT Signal is sent to the TVC and in addition a NIM-pulse is generated. On receiving the EVENT Signal, the TVC locks the TU, thus inhibiting more triggers and reads out the time label and trigger registers.

The NIM-pulse is split and fed into the START inputs of all STAS-Modules. The STAS first sends a signal (LOAD), which moves the data from the comparators into the shift-registers of the front-end boards. Then a clock signal is applied which shifts the data along the chain into the memory of the STAS. Upon completion of the readout the STAS produces a LAM signal which is fed into an external interrupt input of a CAMAC branch driver CBD8210 to generate a VME-Interrupt.

This interrupt signal causes a high priority process of the TVC to scan all STAS and ADC modules for LAM signals and to transfer the data into the memory of the TVC. When this task is completed the TU is unlocked and a low priority process preprocesses the data and sends it, via a second TVC over TCP/IP, to the central event builder that

assembles the data from all detector components of KASCADE according to their time labels.

The high priority Data Acquisition Program (DAQ) coordinates the experiment control, time and event handling and data storage. It uses C-routines on TVC, which initialize the hardware: the VME and CAMAC crates, the Trigger-Unit, the STAS controllers and the ADC modules. For this initialization an experiment set-up file, structured similar to Windows .ini files, is read, which contains the addresses of the crates of the STAS modules and the ADC modules in the the crate and the number of each readout chain for a given STAS module. Readout chains are subdivided in subchains, each corresponding to a group of readout boards for the wires and strips, respectively. The description of the configuration is done in a way that allows maximal flexibility in the actual setup of the experiment.

While the event acquisition is performed with high priority, the data transfer from TVC memory to the central event builder is done with low priority. Monitor histograms of various parameters are also allocated and filled with low priority. These histograms can be viewed online with a separate program that connects to the running DAQ, thus allowing to perform immediate checks when doing adjustments of threshold and timing settings on the frontend boards.

The different datablocks (TU, Stas and ADC data) are combined into one large block and sent to the central event builder, where they are merged with the data coming from the other components of the KASCADE experiment.

The raw data are afterwards analyzed with the help of the program KRETA, which calibrates the hit positions by means of the improved geometry data base (DB).

6 Tests of detector performance

6.1 The events selection

For testing various aspects of the MTD performance the data sample, covering the period from 4th October 1998 to 5th April 1999, has been analyzed. Within the total time of data taking of 4366 hours $8{\cdot}10^6$ events have been collected with $1.5{\cdot}10^6$ tracks reconstructed in the MTD.

The sample of collected tracks is divided into two kinds of configurations: the, so-called, *2-hit* tracks and the *3-hit* ones. The *3-hit* tracks are tracks with hits in three modules, and the track finding algorithm looks first for them. Thereafter, the algorithm looks for the *2-hit* tracks, using for these the hits in two modules, not utilized by the *3-hit* tracks.

6.1.1 MTD data selection criteria

In order to estimate the angular resolution of the MTD and to check its geometry it is necessary to select tracks generated only by high energy muons (E_μ >few tens of GeV). Such muons are produced in the higher slices of the atmosphere, they are nearly parallel and well aligned with the shower direction. Simulations show that muons produced ~ 8 km above sea level and with energy larger than 30 GeV form an average angle with the shower direction of less than 0.3^o. On the other hand, the more important information about the longitudinal development of the showers comes from the higher part of the atmosphere, where, for showers detected with the same number of muons, the heavy nuclei produce a larger number of muons compared with the lighter ones.

However, in the sample of all reconstructed tracks there is a fraction of tracks that is produced by particles with *low* energy (this is due to the limited absorber thickness above the tunnel) and by chance in the reconstruction algorithm. These have to be rejected. From now on these tracks will be called *unwanted* tracks even if some of them are produced by muons.

First of all we have accepted *3-hit* tracks with a normalized χ^2 lower than 2.5. The χ^2 is defined as:

$$\chi^2 = \sum_{i=1}^{3} \frac{D_{tr}^2(Hit_i)}{A_{Hit_i}}$$

where $D_{tr}(Hit)$ is the distance in space between the *hit* and the *track* coordinate and A_{Hit} is the *area* of the hit (*wire cluster size* $\times$ *strip cluster size*). The just defined quantity is not a *standard* χ^2 because we have used the inverse of the area of the hit as a weight of the square of the hit-track distance. But it has the same behavior. This χ^2 cut rejects with high efficiency accidental tracks without reducing the particle track sample.

Fig. 17 shows the correlation between the χ^2 with the distance between the shower core and the tunnel-track. When the distance becomes smaller the flux of particles in the tunnel becomes more intense. This produces a deterioration of the track finding algorithm performance correlated with the increase of the number of hits in the towers. In fact, if the number of hits in each tower increases, it becomes more frequent for the track finding algorithm to find just by chance groups of three hits aligned. Therefore, the number of accidental tracks in the sample increases in correlation with the number of hits in the towers and, consequently, increases the χ^2 value.

For the *2-hit* tracks it is not possible to define the χ^2. In this case a *track-deviation* (S) parameter has been introduced using as reference the direction of the shower axis reconstructed by the array (see fig. 18).

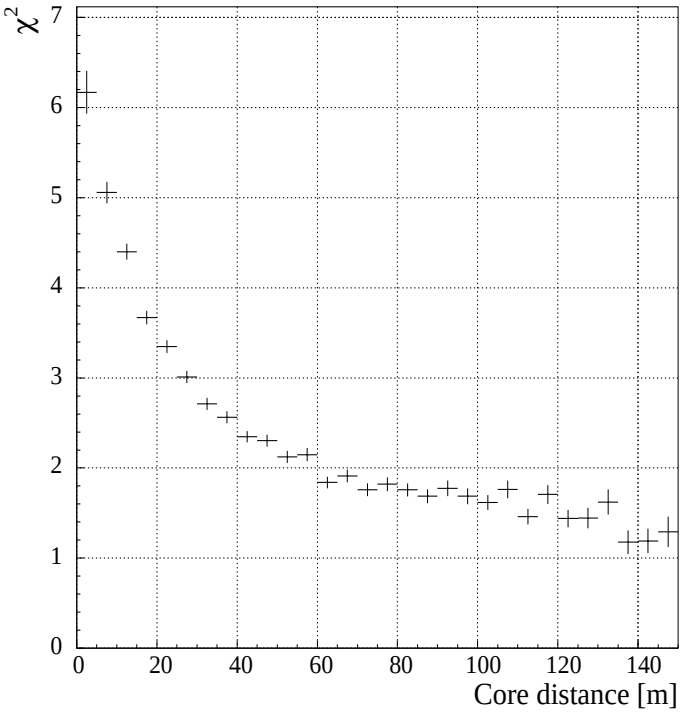

Figure 17: Correlation between the χ^2 of *3-hit* tracks and the core distance.

The tracks with a *deviation* larger than 10 cm ($\sim 7.2^o$) are rejected, which is equivalent (just from a geometrical point of view, taking into account the dimensions of the KASCADE detector array) to rejection of *hard particles* produced below $\sim$ 1,2 km above the detector. It is evident that these two cuts for the two samples of tracks work in a different way. The first one, χ^2 on *3-hit* tracks, eliminates mainly accidental tracks while the second (*2-hit* tracks) rejects also a fraction of soft particles.

Fig. 19 shows the correlation between the angle in space Ψ (defined as the angle between the shower direction and the MTD track) and the distance of the MTD track from the shower core. It is evident that for a distance less than 50 m the contamination of *unwanted* particles is still high and that this contamination is more evident in the *3-hit* tracks, because for them no kind of alignment with the shower is required. Therefore, a distance cut of 50 m has been considered.

6.1.2 Scintillator array selection criteria

The scintillator array of KASCADE plays an important role in our analyses. Therefore, the event selection criteria have to take into account also the performance of the array.

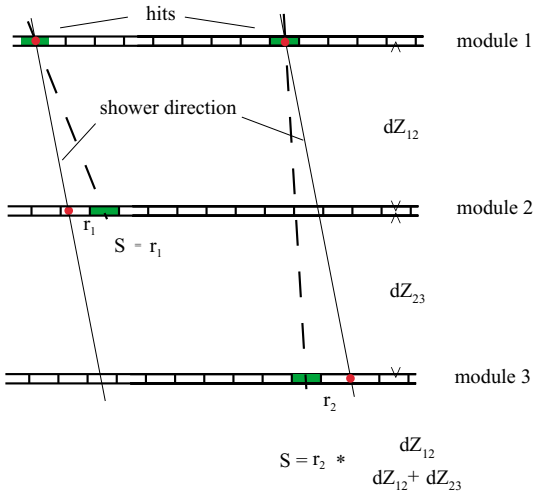

Figure 18: The *track-deviation* (S) is defined as the distance in the detector module of the second hit of the track from the direction in the space identified by the first hit and the shower direction, normalized by the distance between the modules.

For this reason some cuts have been considered to guarantee a good reconstruction of the shower parameters.

We have accepted only events with the core reconstructed in a fiducial area of 90 m around the center of the KASCADE detector array, with a reconstructed *age* in the range $0.2 \div 2.1$ and with a number of triggered photomultiplier tubes of the electron/gamma detector (inner + outer clusters) larger than 9. Moreover, for compatibility with our other analysis we have accepted only events with a truncated number of muons reconstructed by the scintillator array larger than $10^{3.25}$ and with zenith angle smaller than 45^o.

The *electron size* distribution of the showers surviving these cuts is shown in fig. 20. It is peaked at $10^{4.35}$ and the fraction of accepted showers with size lower than 10^4 is below the 10% (curve in the figure). All these criteria guarantee a *good reconstruction* of the shower direction and core position by the array [37].

6.2 The geometry checks

The angular resolution of the MTD is a crucial parameter and it depends on the precision of the determination of the real positions of the wires and strips in the towers. Even if the assembly of the towers has been done carefully, shifts of one module and/or one plane of wires or strips with respect to the other in the same tower are possible. These misalignments cause a deterioration of the detector angular resolution.

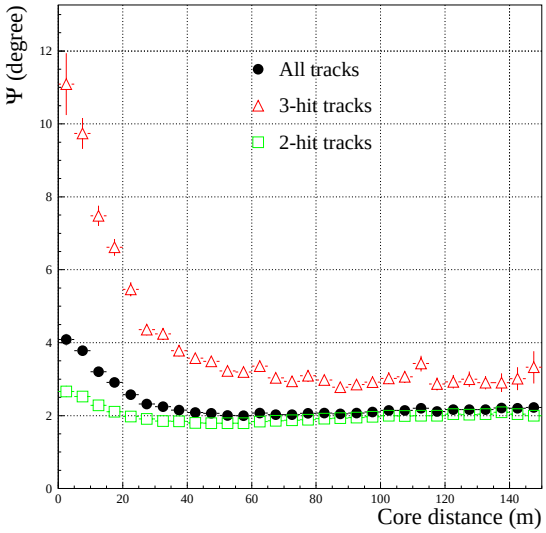

Figure 19: Average angle between the direction of the shower and the track in the MTD versus the distance of the MTD track from the core.

Therefore, it was necessary to design methods of checking the actual geometry of the towers for taking it into account in the course of resolution calculations.

The positions of the strips and wires have been measured using optical and mechanical methods, first with respect to the four corners of the module. Then the positions of the modules were measured with respect to the reference system of the tunnel housing the MTD. This reference system has its origin in the center of the tunnel with the y-axis along the long side and the x-axis along the short side of the tunnel. The z-axis is oriented towards the ceiling of the tunnel. Each of these measurements has a precision of better than 2 mm, therefore, the precision of determination of the wire and strip positions in the tunnel reference system is better than 2.8 mm.

All the coordinates of wires and strips are stored in the *default geometry data base (DB)*. As the direct measurement can be affected by systematic errors in the positioning of the used tools, the geometry has to be verified with independent techniques, involving cosmic muons.

6.2.1 Internal coherence of each module

In the first place the internal coherence of each module has been checked using the diagonal strips. This check has been done using very clear event configurations in which only

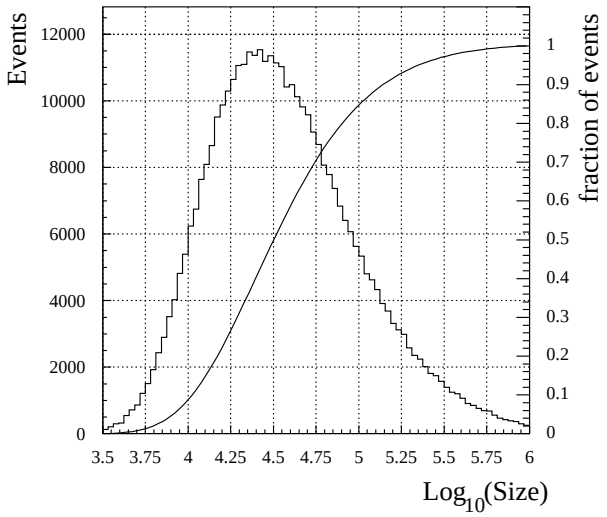

Figure 20: Electron size distribution of the showers surviving the selection criteria (histogram). The curve in the plot shows the integral distribution of the electron size (right scale).

one wire and one strip in both strip planes (*perpendicular* and *diagonal*) have been fired. Assuming that the X and Y positions have been measured correctly one can minimize the distance of any X, Y hit to its closest diagonal strip and improve the *default geometry DB* for the diagonal strips. In this way one has the possibility to identify (and to eliminate) both a systematic offset of the diagonal strip plane with respect to the X, Y hits and a systematic rotation of the diagonal strips plane with respect to its nominal (60.0^o) orientation.

Fig. 21 shows calculated mean values of distributions of distances between the X, Y crossing point and the nearest diagonal strip for 13 towers being in operation at the time of writing this manuscript. Variation of the overall diagonal strip position allows to obtain a narrow distribution centered nearly at zero. Fig. 21 shows, that the distributions for all modules in each tower are not yet fully centered at zero but are in some cases off by a few millimeters. There remains certain staggering of the displacement, which is observed to be correlated with the orientation of the diagonal strips in the modules and which has to be further investigated.

6.2.2 Alignment checks with cosmic ray particles: 1st method

The first method, commonly used for verification of the geometry of a tracking apparatus, consists in using the residuals of the fits of the cosmic muon tracks. The residual in one view (wire or strip) is defined as the difference between the hit position in that view and the position at which the reconstructed track crosses the module in this view.

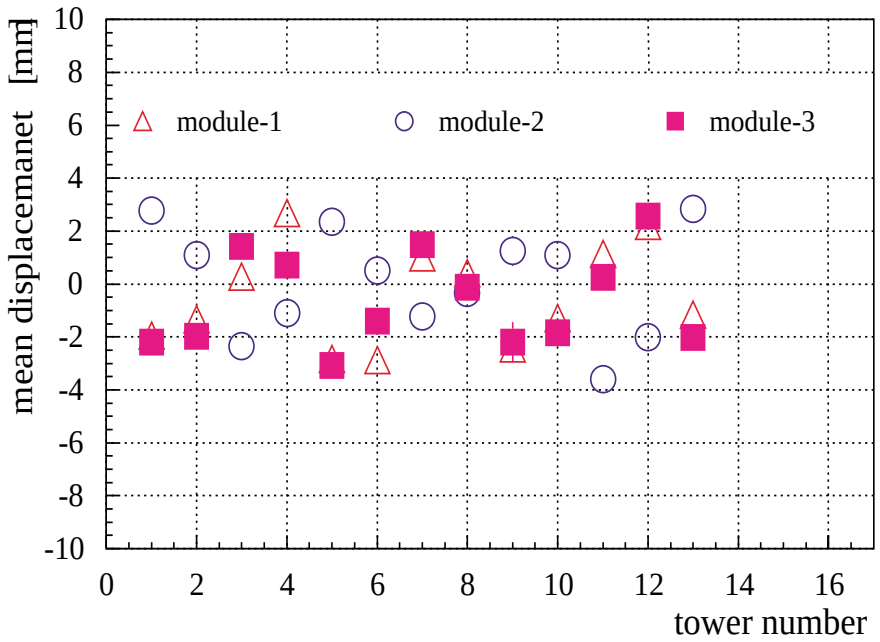

Figure 21: Calculated mean values of distributions of distances between X, Y crossing point and the nearest *diagonal strip* for 13 towers

The RMS of this distribution in the different views gives the uncertainty in the position of the detector modules. Moreover, the residual distribution can be also used for fine tuning of the geometry itself and then for building an *improved geometry DB*. This is an iterative procedure which, in several steps, allows to correct the positions of the modules by bringing the peak position of the residuals to zero.

The potential of this method cannot be fully utilized in the specific case of the KASCADE muon tracking detector because, at present, there are only 3 modules for the determination of a track. In fact, it is possible to run into a systematic tilt of a tower. If, for example, the *correct* track is vertical, but the bottom module (3rd) in the *default geometry DB* is shifted to the right, then one goes into ambiguity. Two indistinguishable solutions are possible: either to shift the 3rd module to the left (correct) or to shift the 2nd module to the right (wrong).

However, this method can be used to reduce the spread of the distribution of the residuals and to improve the intrinsic angular resolution without *changing* the reconstructed direction of the tracks. It can be applied to *shift* only one module, e.g. the middle module, in each tower using the top and the bottom to fix the particle direction. The possible systematic tilt of the towers has to be checked and (if necessary) eliminated with other techniques. Such a technique could consist in finding for all towers a most identical angular

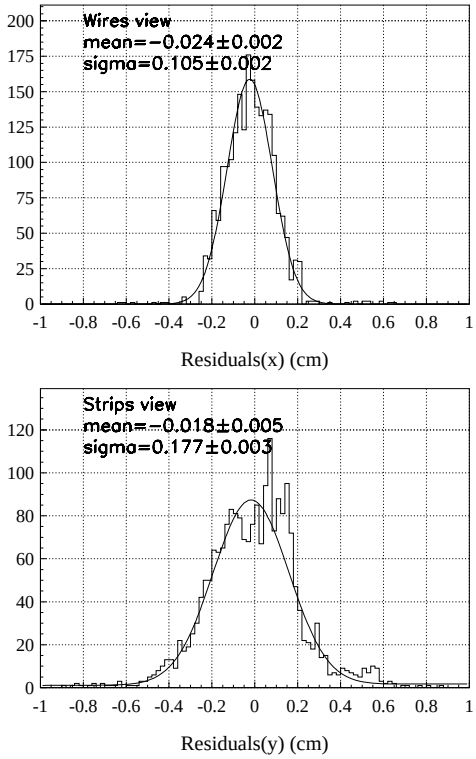

Figure 22: The residual distributions for the middle module (2nd) in the two views, applying the method in 6.2.2. The top panel shows the X-view while the bottom panel shows the Y-view.

distribution in zenith and azimuth angles for cosmic ray particles penetrating the towers. Another technique could employ a well aligned plastic scintillator telescope with fixed orientation inside the tower confining tracks to a well defined angular range and centroid angle. So far, the technique described in section 6.2.3 was employed.

Fig. 22 gives an example of application of the procedure described in section 6.2.2. For the analysis the data taken with eight towers available at that time of detector build-up have been used. The residual distributions obtained for the middle module of all those towers together in the two views are shown. The RMS of the distributions represents a value of the uncertainty in the geometry of the towers determined by data analysis.

6.2.3 Checks with cosmic ray particles and scintillator array: 2nd method

A modification of the previous method, that can be adopted in the case of KASCADE, consists in using the direction of the reconstructed shower from the scintillator array. In this case only one module is needed (the middle one) for track identification (because the direction is fixed by the shower axis). Next, the distributions of the residuals in the different views of the top and bottom modules are analyzed.

In comparison with the first method (section 6.2.2) this one can be used to check, whether a systematic inclination of the towers is present, therefore, it allows to check the accuracy of the full tracking detector in *pointing the sky*. Application of this method requires taking into account physics of the extensive air showers. In high energy interactions at the top of the atmosphere the secondary particles are produced with a certain transverse momentum (P_t). Therefore, directions of muons, created in the in-flight decay of secondary pions and kaons, exhibit angles with respect to the direction of the shower axis. This angle can be used to reconstruct the MPH [4]. Possibly, one can also investigate model predictions concerning the transverse momentum distribution in very high energy interactions.

At the same time P_t acting in every hadronic interaction along the shower cascade, introduces a systematic modification of the zenith-azimuth distribution of the muon directions, with respect to the shower directions. This is a symmetric effect in the shower reference system. To conserve the circular symmetry in application of this second method, only reconstructed showers in a circular area around each tower should be chosen. Moreover, the distribution of the shower core positions in this ring area should be uniform.

The advantage of this technique with respect to the first method is, that it allows to eliminate the ambiguity mentioned above (see section 6.2.2). Moreover, it allows to check the alignment of the towers with respect to the scintillator array.

The disadvantage is that, because of the geometry of the KASCADE setup, for this analysis it is not possible to use the core distance cut (>50 m) and still have the uniform distribution of shower core positions in the ring area around MTD. Therefore, the obtained distribution of the residuals can be very wide.

Another source of uncertainty is the accuracy in the reconstruction of the shower direction from the scintillator array. Systematic errors, dependent on the position of the core of the shower inside the array, can simulate misalignment between the two detectors.

Fig. 23 shows an example of application of the method. The distributions of the residuals in the two views for the top and bottom modules obtained for a group of 8 towers are shown.

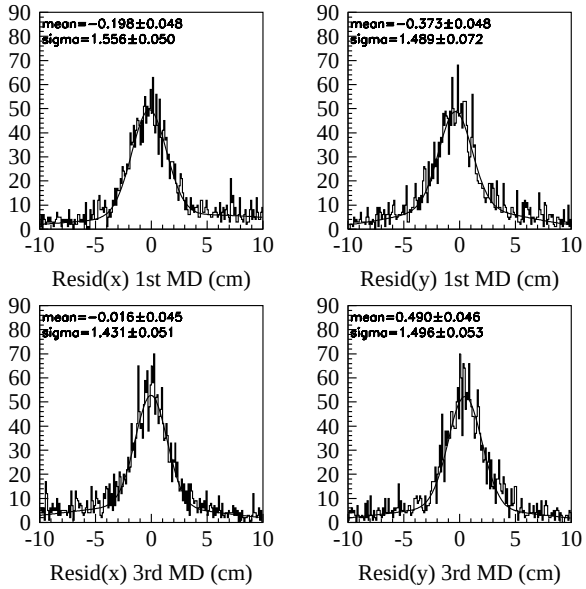

Figure 23: The residual distributions for the top module (1st) (upper panels) and for the bottom module (3rd) (lower panels) in the two views, applying the method described in 6.2.3.

From such distributions a *tilt* angle of the MTD with respect to the scintillator array can be deduced. At the example shown it amounts to 0.3^o in the Y view and $< 0.1^o$ in the X view. The misalignment in the Y view is too large to be compatible with the direct measurement of the module positions done using mechanical tools (~ 3 mm $\Rightarrow \sim 0.1^o$) while the misalignment in the X view is within the errors of the measurement. Then, these 0.3^o might be a result of a systematic tilt as discussed in 6.2.1. This example shows how the described method can be used to subsequent mutual tuning of both detector systems in the KASCADE experiment.

6.3 Angular resolution

The investigation of the various aspects of angular resolution of the MTD is discussed in the following chapters. Several methods of its estimation are presented.

6.3.1 Intrinsic angular resolution

The tracking detector has a *geometrical* resolution which is mainly defined by the dimensions of the streamer tube strips (20 mm) and the separation of the modules in the towers (1640 mm). This resolution is known with certain errors, due to finite accuracy of the geometry determination (see 6.2). Full *intrinsic* resolution, which can be achieved by MTD in determination of the muon directions, has to take into account also other factors.

Based on detailed MC calculations an estimation of the full resolution and its dependence on the zenith angle has been obtained using a simulation of the MTD [36], that takes into account its geometry and physical processes connected with the interactions of the particles in different materials that build up the detector including the tunnel shielding. Fig. 24 shows the angle between the true muon direction and the reconstructed one and its dependence on the zenith angle, obtained with CRES (Cosmic Ray Event Simulation) Monte Carlo program. CRES is a GEANT3 based code.

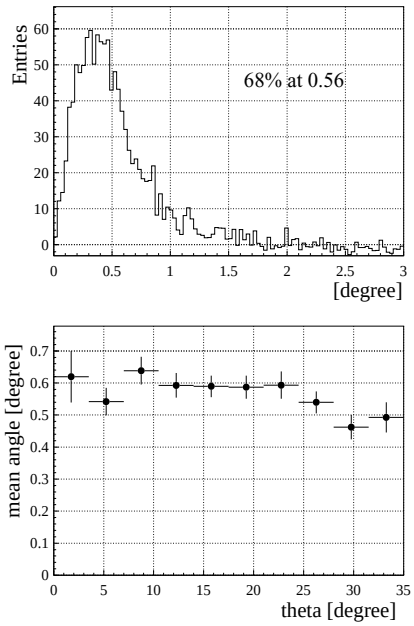

Figure 24: Intrinsic angular resolution of the tracking detector, obtained with a detailed simulation (top), and its dependence on the zenith angle (bottom).

The sample of muons used as input particles for the code has been chosen in such a way, that it reproduces the zenith and the azimuth distributions of the showers reconstructed by the scintillator array with a realistic energy spectrum [35].

Moreover, to simulate the uncertainty in the geometry of the detector, two different *geometry DB* are used, one for the simulation of the events and another for the reconstruction of the tracks. The second *geometry DB* has been obtained starting from the first one and smearing the positions of each module randomly with a sigma of 3 mm.

The angular resolution of the tracking detector obtained as the 68% of the distribution of the angle between the real muon direction and the reconstructed one is 0.56^o (see fig.24 top panel). This value can be assumed as the intrinsic angular resolution of the detector in tracking charged particles. For this value, only tracks with one wire pair and one perpendicular strip group and cluster size equal to one have been considered.

In ideal case, assuming that the geometry is exactly known, this value equals to 0.41^0.

The average value of this angle is dependent on the zenith angle of the tracks (fig. 24 bottom panel), because the effective dimensions for wire cell and strip, as *seen* by the tracks, decrease with the increase of the zenith angle and, at the same time, the distance of flight between two modules in the detector increases with the zenith angle. Compared to the *intrinsic* angular resolution, which one has to assume for the real detector, it is also to be remembered that the MC calculations, which consider bigger clusters size and crosstalk in the electronics, may worsen the quoted figures.

6.3.2 Total angular resolution in pointing the sky: two muons

A commonly used method to determine the total angular resolution in the pointing of a MTD consists in measuring the angle between two tracks. This approach is based on the idea that on average the high energy muons in a shower can be assumed to be nearly parallel. This assumption is not fully valid because muons in a pair may originate from different production heights and may, therefore, not be quite parallel. Furthermore most muons in our data sample have energies near to the detector threshold (around 1 GeV). Nevertheless, this hypothesis allows to investigate the influence of various parameters which enter into the analysis on the quality of this angular resolution.

In our case this technique allows to test the orientation of individual towers with respect to the others and it is not influenced by eventual systematic errors or asymmetries in the reconstruction introduced from the array. The drawback is that a large statistical sample is needed and that the method cannot be used to correct the towers alignment but only to verify it. In fact, it is not possible to identify which of the two towers is wrongly aligned and one can only align all the towers with respect to one of them.

To illustrate the potential of this method a result from the analysis of a sample of data taken with not fully tuned tracking detectors (9 towers) is shown in fig. 25. In the track

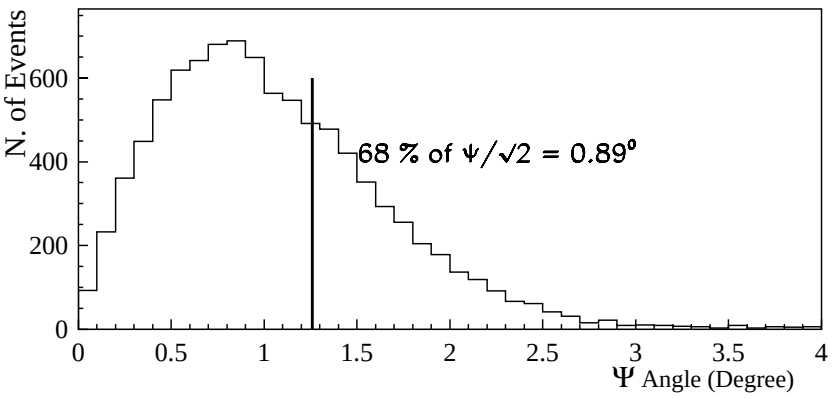

Figure 25: Angle (Ψ) between two tracks in the tracking detector. One of the tracks has to be in the tower 9.

analysis software routines one distinguishes between tracks which are derived from hits (hits are individual wire-strip crossings) in any 2 modules: *2-hit* tracks and tracks, which are derived from hits in 3 different modules: *3-hit* tracks. The cut used for this analysis selects events in which there are only two *3-hit* tracks in the full detector with no more than one track in each tower. No restriction on the cluster size of the hits was used.

In fig. 25 the angle in space (Ψ) between the direction of two tracks in our tracking detector is plotted. One of the tracks was required to be in tower 9. In this way tower 9 (center of the tunnel) has been used as the reference tower and the alignment of all the other towers has been checked with respect to it. The total angular resolution of the detector defined as the angle containing the 68% of the events divided by the $\sqrt{2}$ is 0.89^o.

This obtained angular resolution is the combination of the intrinsic resolution of MTD and of the effects of multiple scattering of the muons in the atmosphere, as well as possible effects of differences in the production heights.

6.3.3 Total angular resolution in pointing the sky: the tangential angle

In a cylindrically symmetric problem, which we meet in the case of a high energy air shower accompanied by secondary particles, it is natural to consider the *radial* and *tangential* angles. In particular using the *tangential* angle (τ) can be another method for the determination of a total angular resolution of the tracking detector in cosmic ray applications.

This variable is defined in [34] as the angle between the muon track and the projection of the muon track on the *radial* plane. This plane is subtented by the shower axis and

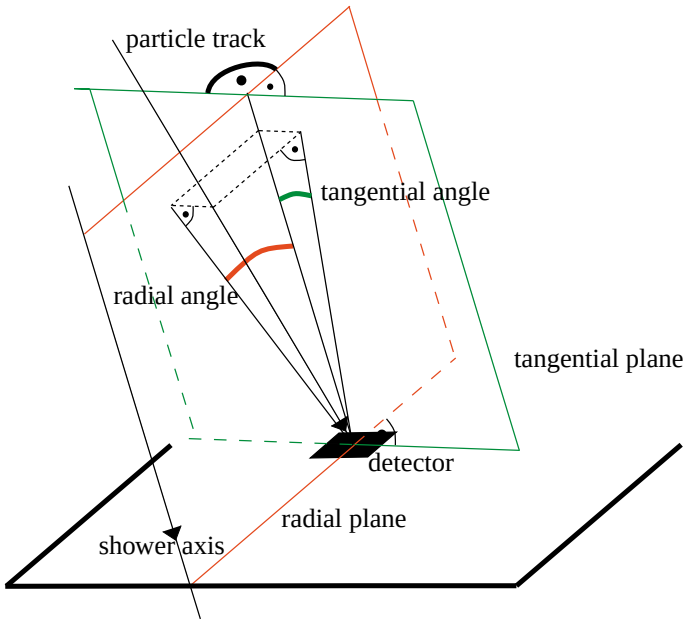

Figure 26: Definition of *radial* and *tangential* angles between the shower axis and the measured track of a particle.

the line connecting the shower core and the hit position where the muon crosses the array detection plane (see fig. 26).

The tangential angle introduces some interesting advantages. It is symmetric around zero (if no systematic effects are present in the MTD or the array). In fact, the spread of this distribution depends on the multiple scattering of the muons and on the resolution of the two detectors, as well as on the transversal displacement of the muon origin (all are symmetrical processes). However, each tangential angle value for each muon in a shower is a function of the relative position of the shower core and muon. Therefore, any shift of its distribution from zero, depending on the relative position, is an indication of some kind of systematic effect in the *array/tracking detector* reconstruction and can be used for mutual tuning of both detectors.

6.3.3.1. Correlation between the tangential angle and the angular resolution
The following simple equation can be assumed to convert the RMS of the tangential angle distribution (σ_τ) to the angular resolution for a direction in the space: $\sigma_\Psi = \sigma_\tau \cdot \sqrt{2}$.

This formula is the standard relation between the σ of a two-dimensional gaussian distribution and the σ of its projection on a plane. It has been checked by simple MC simulation how this relation holds in our experimental conditions. For the simulation, the

direction of experimental showers was taken as direction of two tracks. The first track was taken as a shower axis, the second track as muon track. The position of the first track in each simulated event has been flat distributed on the scintillator array (shower axis), the position of the second track has been distributed on the detectors in the tunnel (muon). The two tracks (initially parallel) are then independently tilted to simulate a resolution of known RMS. Then, the tangential angle has been calculated. In this way it is possible to estimate the correlation between the known angular resolution introduced and the RMS of the tangential angle.

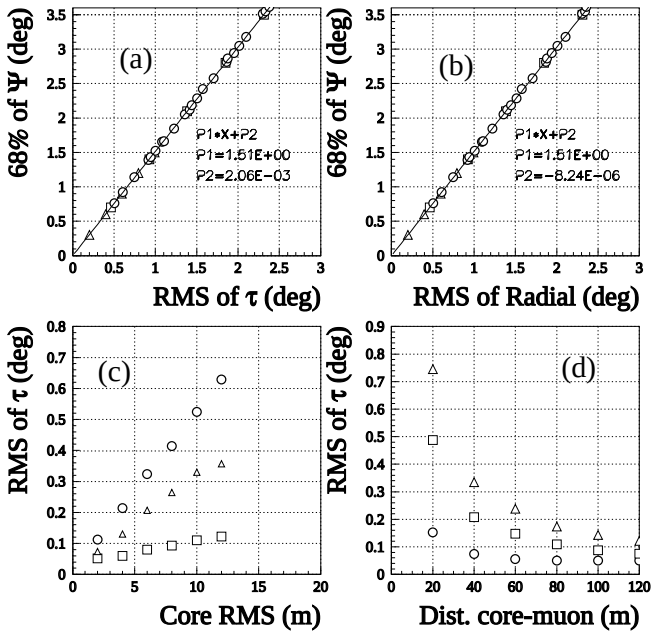

Figure 27: The plot **a**(**b**) shows the correlations between the tangential(radial) angle RMS and the simulated RMS of the shower direction (triangles), muon direction (squares) and combined one (points). Plot **c**: the points have been obtained for radial angle of 3.5^o; the triangles for 2.1^o; the squares for 0.7^o. Plot **d**: points obtained with a core RMS of 2 m; squares for core RMS of 6 m; triangles for core RMS of 10 m (for all these sets a radial angle of 2.1^o has been assumed).

In fig. 27 (plot **a** and **b**) the correlation obtained and the results of a linear fit are shown. The results show a discrepancy ($\sigma_\Psi = 1.51 \cdot \sigma_\tau$) with the more general case of the

above mentioned equation ($\sqrt{2} = 1.41$). The reason for this small discrepancy should be investigated.

With the same Monte Carlo it is also possible to evaluate the uncertainty in the tangential and radial angle calculation introduced by the error in the reconstruction of the shower core position. Fig. 27 shows, that this uncertainty is very small (plot **c**) and it is correlated with the distance between the tracks (plot **d**). Moreover, the correlation between the error in the shower core reconstruction and the spread of the tangential angle distribution changes with the radial angle (plot **c**, different symbols). For larger radial angles the tangential angle is more sensitive to the precision in the shower core reconstruction. Therefore, in our analysis we have accepted only events with the distance between shower core and muon track >50 m. This cut guarantees that the uncertainty in the tangential angle is below 0.3^o.

6.3.3.2. Total resolution and tangential angle The tangential and radial angles can be defined also between two muons in MTD. This technique has additional advantage, that it allows *to clean* the analyzed sample from *unwanted* tracks (tails in the distribution), still not rejected by the introduced cuts (see above).

If one would plot the tangential angle distribution (τ) between two muons, for the same combination of cuts and towers as introduced in the previous section for the two muon analysis (6.3.2), one would see that the plot shape contains more than one gaussian. This indicates, that in the sample *unwanted* tracks are still present.

Based on this assumption the plot should be the superposition of three gaussians (two muon tracks, one muon and one *unwanted* and two *unwanted*) but, as the contamination of *unwanted* tracks is low, the 3rd gaussian is very difficult to be identified. A double gaussian fit to such a plot allows to find the parameters of the two distributions and to exclude from the sample tracks created by one muon and one *unwanted* particle.

The RMS of the remaining gaussian distribution, converted with the factor $\sqrt{2}$ into angular resolution, gives the estimation of total angular resolution in pointing the sky by the tracking detector, and amounts to 0.94 ± 0.08^o.

6.3.4 Combined resolution of the MTD and the scintillator array

Having within one EAS experiment two independent detectors, being able to reconstruct the direction of the showers, has an important advantage. Namely, one has the possibility to combine the two reconstructions in order to improve the total angular resolution of the experiment.

The main disadvantage of a scintillator array in the reconstruction of the shower direction is that its angular resolution deteriorates with the reduction of the shower size. Moreover, the algorithms adopted are usually developed and tuned with Monte Carlo data and a possible systematic effect, due to an incorrect simulation of the shower time profile in the array stations, cannot be detected by using the array data alone.

The first analyses show, that the resolution of the MTD is only weakly dependent on the shower size. Therefore, it can be very useful to improve the KASCADE resolution at lower shower size and to check the scintillator array resolution in an independent way.

The best way to use the MTD in this context is through the tangential angle τ. This gives the twofold advantage. It reduces the effects correlated with the MPH and, as shown before, helps in the elimination of the *unwanted* tracks, thus improving the resolution of the tracking detector itself.

The tools for such a kind of cross-analysis are still under development.

6.4 Examples of data correlated with the array

6.4.1 Muon lateral distributions

The interest in the muon lateral distributions in EAS comes from the fact, that their shape is one of the primary particle mass sensitive parameters.

Based on the, in average, shorter interaction length of iron nuclei the first interaction of iron primary with the atmosphere takes place earlier, compared to the case of primary proton. Thus, the produced muons spread out more in transversal directions in the air shower, because of their higher place of production. This results, for the same muon number, in smaller muon densities in the shower central region for iron induced showers than in the case of proton initiated ones. In other words, the muon lateral distribution for iron induced showers is flatter than for showers initiated by lighter primaries.

As mentioned above (section 2), the MTD data can be used for determination of muon lateral distributions in EAS, which then can be compared with such distributions obtained with the scintillator array alone for the same shower sample. An example of such a comparison is given in fig. 28.

For a data sample of $\approx$ 26.7 millions of showers, registered by KASCADE between dates: 8.12.1999 and 18.4.2000, muon lateral density distributions with the MTD data were calculated. Only showers with zenithal angle θ<18^o were considered and the plots were made for four truncated muon number $\lg(N_\mu^{tr})$ value ranges between 2.9 and 4.5. This truncated muon number ($N_\mu^{tr} = \int_{r_1=40m}^{r_2=200m} 2\pi\rho_\mu dr$) was found to be a good primary energy

estimator in KASCADE [38]. In the picture symbols show the data points and the lines represent the fits with the NKG function:

$$\rho_\mu(R) = C \cdot \left(\frac{R}{420}\right)^{(s-2)} \cdot \left(1 + \frac{R}{420}\right)^{(s-4.5)}$$

where C and s are parameters to be fit and R is a core distance in [m].

For comparison, fitted distributions obtained with the scintillator array data for the same shower sample are shown (dashed lines). The coloured lines are the fitted distributions of the MTD for the different energy bins. The symbols are measured data for some selected core distances.

Prior to analysing lateral distributions based on MTD data the efficiencies for track determination have to be taken into account. Therefore, for each module of each tower the efficiencies for 2- and 3-hit tracks were calculated and stored.

For muon densities larger than 0.2 $\frac{1}{m^2}$ a correction function is used as the reconstruction efficencies are changing due to the large clusterdepthes.

In every shower event the tracks per tower are counted (including "0-tracks") and the density is calculated taking into account the efficiencies, the effective detector area and the different energy thresholds of the array (230 MeV) and the MTD (800 MeV) . The core distance is not a distance in the plane of the KASCADE experiment but the distance between the shower axis and the track in the tower in the plane perpendicular to the shower axis (shower disc coordinates).

Fig. 28 shows the good agreement between the lateral distributions of muons determined by the array and the MTD. However, the data presented is meant just sa an example of the capabilities of the MTD and can by no means be used for any conclusive statements yet.

6.4.2 Muon production height

Recently Pentchev et al. [39] investigated an integral transformation between the lateral distribution function of the muons and the height distribution of the muon origin (MPH).

Wibig and Wolfendale [40] performed an analytical study of the depth of shower maxima (X_{max}), i.e. the atmospheric depth at which the number of shower particles has a maximum value, as a function of primary energy. This work is based on HEGRA data [41], which determine X_{max} via the lateral density distribution of the shower particles and of the Cherenkov photons.

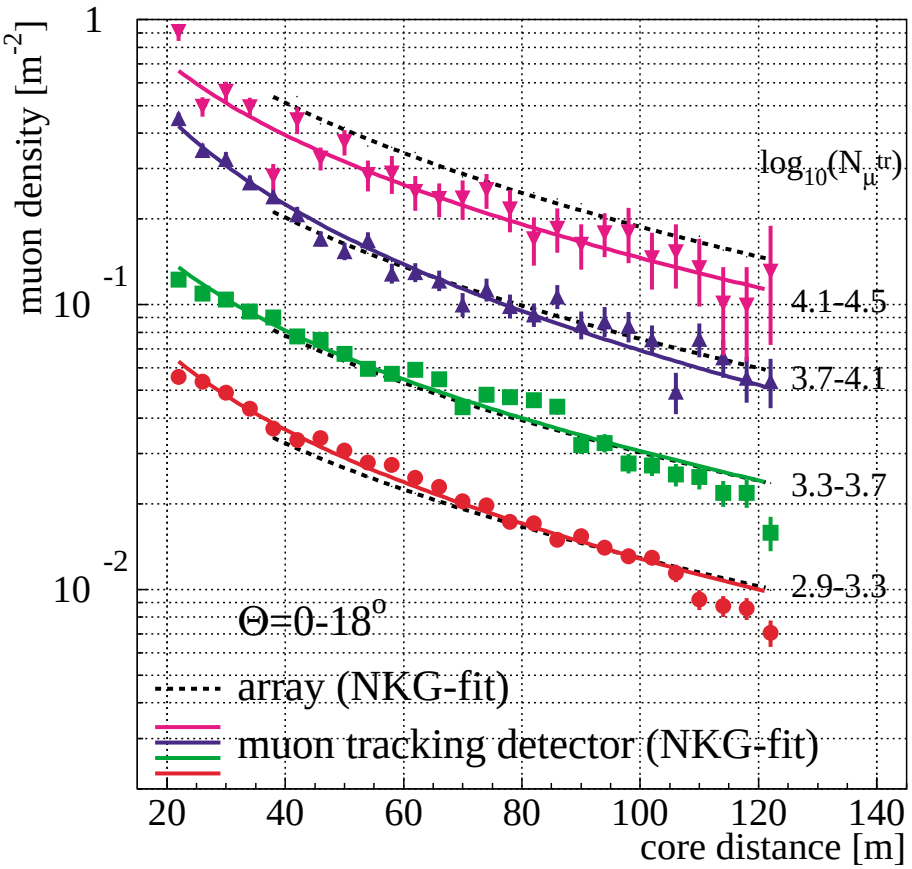

Figure 28: Muon lateral density distributions for four different shower sizes lg(N_μ^{tr}) and zenith angles θ between 0^o and 18^o. Symbols represent data points from MTD and the solid lines, fits to the data. The dashed lines are the fits to the data from scintillation array for the same shower sample.

Similarly, Swordy and Kieda [42] try to derive information on the elemental composition of the primary particles from the *depth of shower maximum in the atmosphere* and the muon and electron sizes at the ground.

The muon production height distributions, built out of the MTD data, for two truncated muon number intervals, corresponding to primary energies around $10^{14.6} eV$ and around $10^{15.9} eV$ respectively, fall in a similar range of atmospheric depths.

The fig. 29 represents for 100 showers in each energy range (incident at a zenith angle around 18^o) the muon track distribution for radial angles between -0.3^o and 5.0^o and tangential angles smaller than 1^o with respect to the shower axis.

Preliminary analyses of the muon production height reveal, that the precision of this technique depends predominantly on the angle and core resolution of the array and the

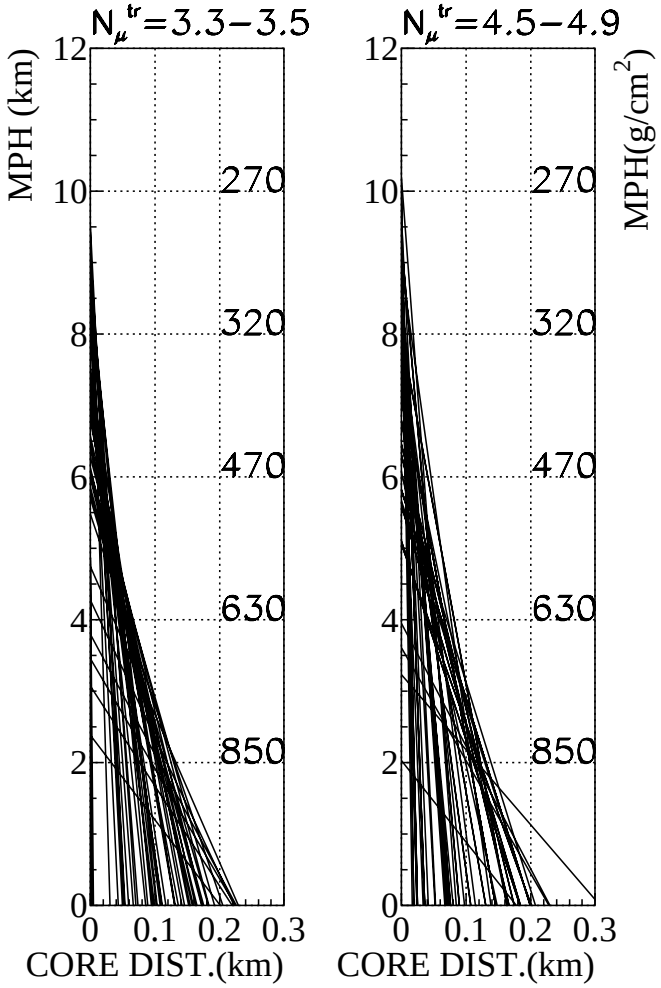

Figure 29: Production height of muons versus distance to the shower core.

MTD. A more elaborated analysis is necessary to excavate underlying features of the nature of the primary particles by means of this technique.

7 Summary

A large area Streamer Tube Muon Tracking Detector (MTD), which has been built within the KASCADE experiment, has the capability to identify muons from Extensive Air Showers (EAS) by track measurements under more than 18 r.l. of shielding. The detector is in the initial stage of its operation and preliminary tests show its satisfactory performance in terms of the stability and track recognition capability.

As presented above, the good performance of MTD has been obtained due to careful design and tests of 1000 ST detectors (specially built for this purpose) and associated electronics.

Further investigations and tuning, both of the hardware and software, are in progress, with the aim to obtain the best angular resolution of the track direction. They use the presented methods of determination of the detector geometry as well as tools for detector angular resolution derivation.

The authors would like to thank the members of the KASCADE collaboration, who contributed to the build up of the muon tracking detector, notably H.Müller.

For valuable discussions and support we would like to thank G.D.Alekseev from Joint Institute of Nuclear Research, Dubna, Russia, M. Meoni from Pol.Hi.Tech, Carsoli, Italy, G. Mannochi and P. Picchi from INFN, Italy, A. King and W. Flegel from CERN, Geneva, Switzerland, L. Pinsky, from University of Houston, USA.

The support from the Ministry for Research of the German Federal Government and from Polish State Committee for Scientific Research (WTZ POL 99/005) is gratefully acknowledged.

References

[1] L. Linsley, J.Phys.G: Part.Phys. **12** (1986) 51;
L. Linsley, Nuovo Cim. **C**15 (1992) 743.

[2] M. Ambrosio *et al.*, Nucl.Instr. and Meth. **A**344 (1994) 350.

[3] M. Ambrosio,C. Aramo,L. Colesanti,A.D. Erlykin,S.K. Machavariani, J.Phys.G: Part.Phys. **23** (1997) 219.

[4] M. Ambrosio *et al.*, Nucl.Phys.(Proc.Suppl.) **75A** (1999) 312.

[5] T.V. Danilova,D. Dumora,A.D. Erlykin,J. Procueur,
J.Phys.G: Part.Phys. **20** (1994) 961.

[6] I.M. Brancus, *et al.*, Astropart.Phys. **7** (1997) 343.

[7] H.O. Klages *et al. (KASCADE Collaboration)*,
Nucl.Phys.B(Proc.Suppl) **52B** (1997) 92.

[8] O. C. Allkofer and P. K. F. Grieder, Physics Data 25-1 (1984) ISSN 0344-8401.

[9] P. Doll *et al.*, Nucl.Instr. and Meth. **A**367 (1995) 120.

[10] S. Ahlenet *et al. (MACRO Collaboration)*, Nucl.Instr. and Meth. **A**324 (1993) 337.

[11] G. Anzivino *et al. (LVD Collaboration)*, Nucl.Instr. and Meth. **A**329 (1993) 521.

[12] J. Gress *et al.*, Nucl.Instr. and Meth. **A**302 (1991) 368.

[13] L. Horton *et al.*, Nucl.Instr. and Meth. **A**325 (1993) 326.

[14] M. Feuerstack *et al.*, Nucl.Instr. and Meth. **A**315 (1992) 357;
W. Rhode *et al.*, Nucl.Instr. and Meth.**A**378 (1996) 399.

[15] O. Catalano *et al.*, Nuovo Cimento. **C**15 (1992) 759.

[16] C. Berger *et al.*, Nucl.Instr. and Meth. **A**262 (1987) 463.

[17] P. Doll *et al.*, Nucl.Instr. and Meth. **A**342 (1994) 495;
P. Doll *et al.*, Nucl.Instr. and Meth. **A**323 (1992) 327.

[18] Pol.Hi.Tech., 67061 Carsoli (AQ), Italy.

[19] D. Hungerford *et al*, Nucl. Instr. and Meth. **A**286 (1990) 155.

[20] G.D. Alekseev *et al*, Nucl.Instr. and Meth. **A**177 (1980) 385.

[21] J.P. DeWulf *et al. (CHARM II Collaboration)*, Nucl.Instr. and Meth. **A**252 (1986) 443.

[22] E. Iarocci, Nucl.Instr. and Meth. **A**217 (1983) 30.

[23] W. Bartl, Nucl.Instr. and Meth. **A**305 (1991) 82.

[24] L. Pentchev *et al.*, Nucl.Instr. and Meth. **A**399 (1997) 275.

[25] Little Falls Alloys, Paterson, NJ 07501, USA.

[26] Steiner Group 57335 Erndtebrück, Germany.

[27] F. Beconcini *et al.*, Trans. on Nucl.Science **35** (1988) 311;
F. Beconcini *et al.*, Nucl.Instr. and Meth. **A**227 (1989) 222.

[28] D. Adams *et al.(SMC Collaboration)*, Nucl.Instr. and Meth. **A**435 (1999) 354.

[29] SGS Thomson Microelectronics, Subsystems, Engineering and R.F.Division, Centro Dorezionale Colleoni, Palazzo ANDROMEDA 3, 20041 Agrate Brianza (Milano),Italy.

[30] MAXIM Integrated Products 120 San Gabriele Drive, Sunnyvale, CA94086.

[31] J. Zabierowski, *et al.*, Nucl.Instr. and Meth. **A**354 (1995) 496;
J. Zabierowski, *et al.*, KfK 5373, (1994).

[32] H. Leich, Transputer based VME Controller-TVC, Internal User Manual, IfH Zeuthen, (1991).

[33] D. Heck *et al.*, Report FZKA 6019 (1998).

[34] K. Bernlöhr, Astropart. Phys. **5** (1996) 139;
K. Bernlöhr, 25th Int.Cosmic Ray Conf.(Durban) **4** (1997) 65.

[35] C. Caso *et al., (Particle Data Group)* The European Physical Journal **C3** (1998).

[36] K. Daumiller, PHD Thesis (2000), University Karlsruhe, in preparation.

[37] R. Glasstetter, PHD Thesis (2000), University Karlsruhe, in preparation.

[38] J. Weber, PHD Thesis (1999), University Karlsruhe.

[39] L. Pentchev *et al.*, J.Phys.G: Nucl.Part.Phys. **25** (1999) 1235.

[40] T. Wibig and A. Wolfendale, J.Phys.G: Nucl.Part.Phys. **26** (2000) 825.

[41] F. Arqueros *et al.*, Astronomy and Astrophysics (2000), in preparation.

[42] S.P. Swordy, D.B. Kieda, Astropart. Phys. **13** (2000) 137.